Modelling atmospheric oxidation of 2-aminoethanol (MEA) emitted from post-combustion capture using WRF–Chem

M. Karl[a, *]

mka@nilu.no

T. Svendby[a]

S.-E. Walker[a]

A.S. Velken[a, b]

N. Castell[a]

S. Solberg[a]

[a]Norwegian Institute for Air Research, NILU, P.O. Box 100, 2027 Kjeller, Norway

[b]Norwegian Environment Agency (Miljødirektoratet), 0663 Oslo, Norway

*Corresponding author at: NILU – Norwegian Institute for Air Research, Instituttveien 18, P.O. Box 100, NO-2027 Kjeller, Norway.

Editor: D. Barcelo

Abstract

Carbon capture and storage (CCS) is a technological solution that can reduce the amount of carbon dioxide (CO_2) emissions from the use of fossil fuel in power plants and other industries. A leading method today is amine based post-combustion capture, in which 2-aminoethanol (MEA) is one of the most studied absorption solvents. In this process, amines are released to the atmosphere through evaporation and entrainment from the CO_2 absorber column. Modelling is a key instrument for simulating the atmospheric dispersion and chemical transformation of MEA, and for projections of ground-level air concentrations and deposition rates. In this study, the Weather Research and Forecasting model inline coupled with chemistry, WRF–Chem, was applied to quantify the impact of using a comprehensive MEA photo-oxidation sequence compared to using a simplified MEA scheme. Main discrepancies were found for iminoethanol (roughly doubled in the detailed scheme) and 2-nitro aminoethanol, short MEA-nitramine (reduced by factor of two in the detailed scheme). The study indicates that MEA emissions from a full-scale capture plant can modify regional background levels of isocyanic acid. Predicted atmospheric concentrations of isocyanic acid were however below the limit value of 1 ppbv for ambient exposure. The dependence of the formation of hazardous compounds in the OH-initiated oxidation of MEA on ambient ~~levels~~ level of nitrogen oxides (NO_x) was studied in a scenario without NO_x emissions from a refinery area in the vicinity of the capture plant. Hourly MEA-nitramine peak concentrations higher than 40 pg m^{-3} did only occur when NO_x mixing ratios were above 2 ppbv. Therefore, the spatial variability and temporal variability of levels of OH and NO_x need to be taken into account in the health risk assessment. The health risk due to direct emissions of nitrosamines and nitramines from full-scale CO_2 capture should be investigated in future studies.

Keywords: 2-Aminoethanol; CO_2-capture; Health risk; WRF–Chem; Nitramines; Isocyanic acid

1 Introduction

Limiting global warming to less than 2 °C relative to pre-industrial levels would require substantial cuts in anthropogenic emissions of greenhouse gases (IPCC, 2014). Carbon capture and storage (CCS) is an important mitigation technology for reducing anthropogenic carbon dioxide (CO_2) emissions from industrial and energy-related point sources. In this process, CO_2 is captured, conditioned, compressed and transported to a storage location for long-term isolation from the atmosphere. Several problems can occur during CCS with impacts on the environment. Post-combustion capture from power plants entails emissions of pollutants, solvents and its degradation by-products to the atmosphere, emissions to water and generation of solid waste (e.g. Reynolds et al., 2012). During the further steps of the CCS chain, CO_2 release during transport in pipelines as well as the escape of injected CO_2 from the storage location to the atmosphere or groundwater pose risks to the environment (Koorneef et al., 2012).

1.1 Use of amines in post-combustion CO_2-capture

Post-combustion capture based on chemical absorption with aqueous solutions of alkanolamines (class of amines which also contains an alcohol group) is one of the most advanced technologies for application in CCS. Among alkanolamines, 2-aminoethanol (MEA) has become a benchmark solvent due to its favourable properties towards CO_2-capture (Vevelstad et al., 2011; Lepaumier et al., 2011; Lepaumier et al., 2009; Puxty et al., 2009). In a full-scale post-combustion capture plant (PCCP) with a capacity of capturing 1 million tonnes CO_2 per year, it is estimated that 40–160 tonnes of amines could be released to the atmosphere (Rao and Rubin, 2002); most realistic is the lower bound (Veltman et al., 2010). An earlier atmospheric worst-case scenario evaluated by Karl et al. (2011) showed that deposition of MEA to small lakes, typical for the Norwegian west coast, may exceed toxicity limits for aquatic organisms. In addition to emissions related to CCS and other industries, alkanolamines have natural sources from oceans and terrestrial vegetation, as they are general products of the biodegradation of amino acids and proteins. Ge et al. (2011a) reviewed anthropogenic and natural sources of amines.

1.2 Health risk assessment of amine-based CO_2-capture

Lee and Wexler (2013) reviewed the primary products forming in the gas-phase oxidation of amines based on available information. Identified gas-phase products include amides, aldehydes, imines, nitrosamines and nitramines. The kinetics of amines and their gas-phase oxidation products have been reviewed by Nielsen et al. (2012) in the context of the health risk assessment of amines from CCS. Nitrosamines are of special concern, as they belong to a class of chemicals that have been shown to be carcinogenic, mutagenic, and teratogenic (Loeppky and Michejda, 1994; IARC, 1982). Nitrosodimethylamine (NDMA) was suspected to be responsible for higher rates of certain cancers in the air around industrialised urban centres (Shapley, 1976). Approximately 90% of the 300 nitrosamines tested have shown carcinogenic effects in bioassays and laboratory animals (NIPH, 2011). Information on health effects of nitramines on humans is scarce. For dimethylnitramine ($(CH_3)_2N\text{-}NO_2$), high carcinogenic and tumorigenic potential has been found (Goodall and Kennedy, 1976; Scherf et al., 1989). Methylnitramine shows carcinogenic potential (Scherf et al., 1989) but no evidence was found for its mutagenic activity (Frei et al., 1984). Recently, the mutagenic potential of the nitramine derived from the oxidation of MEA, 2-nitro aminoethanol (in the following short MEA-nitramine) was confirmed (Fjellsbø et al., 2014).

The risk of contamination of drinking water supplies by nitrosamines and nitramines has been recognized as the most critical environmental impact from amine-based CO_2 capture (Karl et al., 2011; Zhang et al., 2014). In connection with the emission permit for the CO_2 Technology Centre Mongstad (TCM) in Norway, the Norwegian Institute of Public Health (NIPH) established an air concentration limit of 0.3 ng m^{-3} (at cancer lifetime risk < 10^{-5}) for the sum of nitrosamines and nitramines to protect the general population from health hazards in connection with inhalation exposure; and a limit concentration of 4 ng L^{-1} for the sum of nitrosamines and nitramines in drinking water (NIPH, 2011). For comparison, U.S. EPA (U.S. EPA, 1986) recommended a public health goal of 0.07 ng m^{-3} for the air concentration of NDMA at cancer lifetime risk of 10^{-6}. Current regulatory standards for NDMA in drinking water are 3 ng L^{-1} ("Public Health Goal") in California, USA (California EPA, 2006), and 9 ng L^{-1} in Ontario, Canada (Government of Ontario, 2002). In Germany, 10 ng L^{-1} trigger the initiation of remedial actions to reduce NDMA (German drinking water ordinance, 2001).

Karl et al. (2014) developed a model framework that couples the atmospheric chemistry transport model system Weather Research and Forecasting–European Monitoring and Evaluation Programme (WRF–EMEP) and the multimedia fugacity level III model to assess the environmental impact of amine emissions. In a sensitivity analysis towards uncertain parameters of the environmental fate of amines it was demonstrated that realistic amine emissions from a typical PCCP result in levels of the sum of nitrosamines and nitramines in ground-level air (0.6–10 pg m^{-3}) and drinking water (0.04–0.25 ng L^{-1}) below the current safety guideline by NIPH for human health (Karl et al., 2014). However, a number of complicating factors such as the direct emission of nitrosamines and nitramines from the PCCP could not be studied due to lack of information.

1.3 Modelling the dispersion and photo-oxidation of MEA

The main aim of the present study is to investigate the atmospheric product spectrum from MEA-oxidation, including nitrosamines and nitramines but also carbonylic compounds, under different environmental conditions using the detailed MEA photo-oxidation scheme proposed in the work by Karl et al. (2012). The WRF–EMEP model framework included a simplified treatment of the OH-initiated oxidation of MEA intended for prediction of nitrosamines and nitramines, with limited detail on carbonylic products forming upon H-abstraction at the $–CH_2$ and $–CH_2OH$ groups of MEA. In the present study, more details on the formation of carbonylic products were considered. The dispersion of MEA, released from the PCCP, in space and time, with ongoing chemical oxidation, transport, dry and wet deposition, leads to a complex spatiotemporal distribution of the amine and its oxidation products with currently unknown inhalation exposure of the population. Additionally, generated compounds are expected to be hazardous at concentration levels that are currently difficult or impossible to detect and quantify even with most advanced analytical instruments.

The detailed MEA oxidation scheme was integrated into the state-of-the-art model WRF–Chem (Grell et al., 2005) for dispersion simulations with high horizontal and vertical resolution of the lower atmosphere. In the present study model simulation results obtained for July 2007, the month with the highest photochemical reactivity in the region of Bergen, west coast of Norway, ~~were~~ was analysed. According to simulations with WRF–EMEP, the production of MEA-nitramine in the atmospheric oxidation of MEA emitted from the PCCP point source in July corresponds to ~ 60% of the yearly atmospheric production of this hazardous compound. The paper is structured as follows. First, model results of WRF–Chem were compared to results with the WRF–EMEP model using identical model configurations (Section 3.2). Second, the effect of increasing the vertical resolution in WRF–Chem was tested (Section 3.3). Third, the differences between the usage of a simplified versus detailed MEA photo-oxidation scheme were studied (Section 3.4). Fourth, the sensitivity of hazardous product concentrations towards ambient NO_x levels was studied (Section 3.5).

2 Methodology

2.1 Description of WRF-–Chem model setup

The WRF-–Chem model (Grell et al., 2005) consists of a mesoscale meteorological model (WRF) inline coupled with a chemistry module. Atmospheric transport of chemical species and moisture variables is computed inline through the Advanced Research WRF (ARW), using a spatially 5th order evaluation of the horizontal fluxes and a 3rd order representation of the vertical flux divergence coupled to a Runge–Kutta time integration scheme. The equations are formulated using a terrain-following hydrostatic-pressure vertical coordinate and staggered horizontal grids (Skamarock and Klemp, 2008). In this study, WRF-–Chem version 3.4.1, modified to include chemistry and deposition of amines, has been used. The modules and meteorological physical schemes selected in this study are listed in Table 1. The overhead ozone (O_3) column is calculated by the global Oslo CTM2 model as described by Hodnebrog et al. (2012). Meteorological initial and boundary conditions (ICs and BCs) are taken from European Centre for Medium-Range Weather Forecasts (ECMWF) global atmospheric reanalysis (Dee et al., 2011) at a resolution of 0.75~~degrees~~° and updated every 6 ~~hours~~h. The meteorological ~~parameters~~ parameter temperature, humidity and horizontal winds are nudged towards the ECMWF data every time step.

Table 1 WRF-Chem setup: physical and chemical options.

Physical and chemical processes	Applied scheme/setting	Reference/comment
Shortwave radiation	RRTMG	Iacono et al. (2008)
Longwave radiation	RRTMG	Iacono et al. (2008)
Microphysics	Morrison et al. scheme	Morrison et al. (2009). Bulk two-moment scheme that predicts mixing rations and number concentrations of cloud droplets, cloud ice, rain, snow and graupel.
PBL processes	Mellor-Yamada-Janjic (MYJ),	Janjic (2002)
Land-surface	Noah Land Surface Model	Chen and Dudhia (2001). Unified NCEP/NCAR/AFWA scheme with soil temperature and moisture in 4 layers, fractional snow cover and frozen soil physics.
Cumulus	Grell-3	Improved version of the Grell-Devenyi scheme (Grell and Devenyi, 2002). Only applied in the inner domain (2-km resolution grid).
Cumulus radiation feedback	Included	Feedback from the parameterized convection to the radiation and photolysis schemes turned on.
Photolysis scheme	Fast-J	Wild et al. (2000)
Gas-phase chemistry mechanism	RACM	Stockwell et al. (1997)
Cloud chemistry	None	—
Aerosol module	None	—

The Regional Atmospheric Chemistry Mechanism (RACM; Stockwell et al., 1997) was selected for atmospheric chemistry, containing 237 chemical reactions and 77 chemical species. All photolysis rates were calculated with the computationally efficient Fast-J scheme (Wild et al., 2000; Barnard et al., 2004). Fast-J scheme computes photolysis rates online from the predicted O_3, aerosol, and clouds following a Legendre expansion of the exact scattering phase function. Initial and boundary conditions of the chemical species are updated every 6 ~~hours~~h from results obtained with the Oslo CTM2 (Søvde et al., 2008). Since the chemical schemes of CTM2 and RACM differ with respect to the number and accounting of individual non-methane volatile organic compounds (~~NMVOC~~NMVOCs), the NMVOC species in the Oslo CTM2 had to be mapped to the appropriate RACM species. Dry deposition velocities of trace gases are calculated using a series resistance approach following the parameterization by Wesely (1989).

The calculation of biogenic emissions of isoprene and monoterpenes is done online based on the description of Guenther et al. (1995). Anthropogenic emissions of carbon monoxide (CO), nitrogen oxides (NO_x = NO + NO_2), and NMVOC are based on the TNO-MACC emission inventory (Kuenen et al., 2011) which has a spatial resolution of 1/8 degree longitude × 1/16 degree latitude (i.e. about 10 km × 7 km). Interpolation routines developed by Hodnebrog et al. (2012) were applied for redistribution of emissions to the WRF-–Chem model grids. The routines also split the aggregated NMVOC in TNO-MACC into individual VOCs and lumps them again to fit the RACM compounds. The TNO-MACC dataset is divided into 10 emission categories (Selected Nomenclature for Air Pollution, SNAP, categories) with vertical distribution and factors to account for diurnal, weekly and monthly variations associated with each SNAP category (Simpson et al., 2012). NO_x-emissions in the Mongstad grid cell were updated with the correct amount of pollutant release (1930- tonnes NO_x per year) from the European Pollutant Release and Transfer Register.

Precipitation in the western coast of Norway is mainly large scale and the moisture can have its origin far away in the south western North Atlantic (Stohl et al., 2008). A relatively high horizontal resolution is important in complex terrain, such as the Norwegian coast and the mountains, where precipitation has a large orographic enhancement. Convective precipitation for horizontal resolution on a scale of less than 5 km was turned off, since the underlying assumptions for the implicit parameterizations in convective schemes are questionable for high resolution (Hong et al., 2010). Hence, all precipitation processes in this study have been solved using the Morrison two-moment microphysical scheme (Morrison et al., 2009). Heikkilä et al. (201~~1~~0) showed that regional climate simulations for the time period 1961–1990 with the WRF model driven by the ERA-40 reanalysis better resolved the orographic lifting with 10-km horizontal resolution than with 30-km horizontal resolution. Karl et al. (2014) analysed precipitation

data for 2007 at 14 meteorological stations in the region of Bergen, concluding that the WRF model, using identical configurations and meteorological boundaries as in the present study, underestimated the observed precipitation amount on a weekly basis at most stations by up to a factor of two. However, the weekly pattern of observed precipitation was well reproduced.

In order to reduce the computational burden of the WRF-Chem runs, the aqueous phase and aerosol options were deactivated. Including for example an aerosol schemes with 8 size bins adds 88 species that have to be advected, which is computationally expensive both in terms of cycles and memory (Gustafson et al., 2005). Moreover, the main interest was to study the gas-phase oxidation products of amine-related species, involving the need to include new chemical gas-phase species that are advected.

2.2 Simulations and model configurations

A baseline configuration was set up for both WRF-Chem and WRF-EMEP models (simulation Base) to facilitate comparison of the new results with the WRF-EMEP model framework (Karl et al., 2014) that was applied for the same region and year. In addition, three simulations were performed with WRF-Chem, involving (1) variation of vertical resolution (simulation HiVert), by using 37 vertical model layers; (2) variation of MEA chemistry scheme (simulation DetailMEA), by using the more detailed MEA photo-oxidation scheme MEA-Detail (see Section 2.3); and (3) variation of NOx emissions (simulation NoRefNOx) by switching off NO_x emissions from Mongstad refinery. In short, differences between simulations HiVert and Base indicate sensitivity to vertical resolution, differences between simulations DetailMEA and HiVert indicate sensitivity to MEA chemistry description, and differences between NoRefNOx and DetailMEA indicate sensitivity to NO_x emissions. Table 2 summarizes the model configurations used for the baseline and sensitivity simulations. Dry and wet deposition of MEA and related oxidation products is described in section S1 of the Supplementary materials.

Table 2 WRF-Chem simulations: meteorology, specific emissions and chemistry.

Model component	Base		HiVert	DetailMEA	NoRefNOx
	WRF-EMEP	WRF-Chem	WRF-Chem	WRF-Chem	WRF-Chem
Meteorology	WRF	WRF (coupled w/chemistry)	WRF (coupled w/chemistry)	WRF (coupled w/chemistry)	WRF (coupled w/chemistry)
Meteorological ICs and BCs	ECMWF	ECMWF	ECMWF	ECMWF-IFS	ECMWF
Vertical layers total/PBL [a]	20/7	20/7	37/13	37/13	37/13
Top of Atmosphere	100 hPa		50 hPa		
Horizontal resolution outer/intermediate/inner nest	50 km/10 km/2 km	-/-/10 km/2 km	-/-/10 km/2 km		
Data assimilation	FDDA and SST	FDDA			
Point source emissions	Vertical profile: SNAP cat. 9				
Mongstad cell NOx emissions	Total 1930 t per year. 100% NO			Total 1930 t per year. 100% NO	90 t per year (only CCP). 100% NO
MEA chemistry	MEA-simple[b] (Karl et al., 2014)			MEA-detail[b] (Karl et al., 2012)	

[a] PBL height defined with 850 mb pressure level at top.

[b] See Section 2.3.

A coarser outer model domain with the geographic extent of southern Scandinavia at a 10-km horizontal grid resolution, and an inner domain (200 × 200 km^2) with a 2-km horizontal grid resolution (inner domain see inset in Fig. 1) were used in the WRF-Chem simulations. A nest factor of 5 is used in this work to obtain a resolution of 2 km in the inner domain. Although a nest factor of 3 has been more tested, both 3 and 5 are possible nest factors for use in the WRF ARW model (WRF ARW, 2014). Handling of explicit up/down drafts in the Cumulus scheme in the WRF model is very weak if the resolution is over 4 km. Hence, the Cumulus scheme was turned off on the 10-km resolution grid while it was active on the inner nest on the 2-km resolution grid. One-way nesting is applied in WRF-Chem simulations with two grids integrating concurrently, hence initial and lateral boundary conditions for the finer-grid run are obtained from the coarse grid, together with input from higher resolution terrestrial fields (e.g. terrain, and land use, etc.), and masked surface fields (such as soil temperature and moisture). The applied one-way nesting algorithm involves that any air masses that exit the inner domain and then re-enter will have lost the original influence of the inner domain. WRF-Chem is run with extra nudging terms for horizontal winds, temperature and water vapour. Surface-analysis nudging (FDDA) was done in the WRF-Chem Base run and sensitivity simulations.

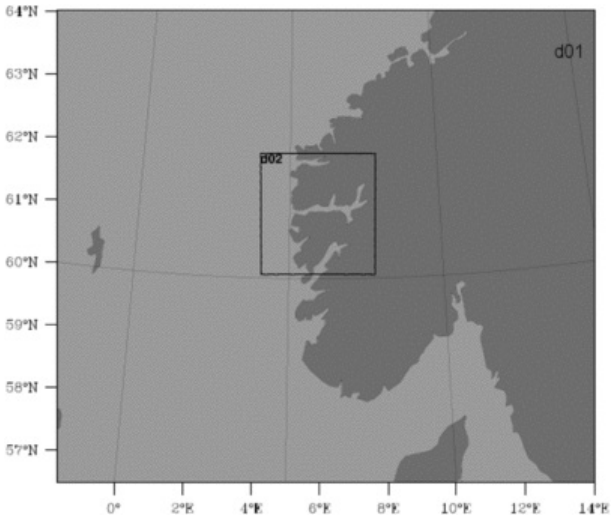

Fig. 1 The modelling domains in the WRF-Chem simulations at 10-km resolution (d01) and 2-km resolution (d02) over southern Scandinavia.

The WRF–EMEP model system developed at the Norwegian Institute for Air Research (NILU) combines WRF with the EMEP MSC-W chemical transport model (Simpson et al., 2012). The system is similar to the EMEP4UK modelling system (Vieno et al., 2010) which is designed for scientific and policy studies in the UK at 5-km horizontal resolution. A detailed description of the configuration of NILU's WRF–EMEP model system is given in Karl et al. (2014). WRF–EMEP applies a one-way nested procedure with separate runs for the different nests, beginning with the coarsest horizontal resolution of 50 km (EMEP standard domain covering all of Europe), an intermediate domain with 10-km resolution and an inner domain with 2-km resolution covering the west coast of middle Norway (200 × 200 km^2); similar to the WRF–Chem inner domain. Upper-air analysis nudging was employed (FDDA) in the nested domains, and time-varying SST (0.5 ~~degrees~~ degree resolution) was employed as input to the model. Meteorological ICs and BCs were taken from ECMWF reanalysis.

Point source emissions from the power plant equipped with full-scale PCCP (as a fictive installation) were distributed over the 2 × 2 km^2 grid cell of Mongstad in the model, entailing 40,000 kg MEA per year and 90,000 kg NO_x (emitted as nitrogen oxide, NO). The vertical distribution of power plant/PCCP emissions was according to SNAP category 9 (Waste treatment and disposal). The vertical profile of SNAP cat. 9 has been shown to approximately match the vertical profile calculated online based on local meteorological data, using common plume-rise parameterizations (Karl et al., 2014). Emissions of MEA and NO from the PCCP were distributed accordingly over the vertical layers in the low vertical resolution (simulation Base, total of 20 vertical layers) and high vertical resolution (total of 37 vertical layers) simulations to match the vertical profile of SNAP category 9. The vertical profile of NO emissions from the refinery at Mongstad was approximated with SNAP cat. 1 (combustion in energy and transformation industries). Table 3 summarizes the vertical profile of emission rates of MEA (from power plant/PCCP) and NO (from power plant/PCCP and refinery) at Mongstad for WRF–Chem simulations Base and HiVert.

Table 3 Vertical emission profile of MEA and NO from both refinery and power plant equipped with CCP at Mongstad [60°48′28″N, 5°02′14″E; 20 m a.s.l.] and total emission amount. Emissions from the 2 × 2 km^2 grid cell of Mongstad are given in unit mg ~~-~~m^{-2} ~~hr~~h^{-1}. Emission profiles are given for simulations WRF-Chem Base (20 vertical layers) and WRF-Chem HiVert (37 vertical layers). Simulation NoRefNOx includes only NO emissions from the power plant equipped with CCP. The vertical emission distribution of MEA in WRF-Chem simulations NoRefNOx and MEADetail is the same as for simulation HiVert. The vertical emission distribution of NO in MEADetail is the same as for simulation HiVert.

Base			HiVert			NoRefNOx
Height (m)[a]	MEA	NO	Height (m)	MEA	NO	NO
0–92	0.114	0.331	0–14	0	0	0
			14–39	0	0	0
			39–91	0.143	0.128	0.128
92–184	0.171	0.331	91–119	0.143	0.128	0.128
			119–175	0.228	2.631	0.193

184–324	0.456	4.353	175–257	0.228	2.631	0.193
			257–318	0.133	13.767	0.698
324–522	0.399	25.033	318–443	0.133	13.767	0.698
			443–564	0.133	8.260	0.530
522–781	0 (align right)	15.781	564–686	0	8.260	0
			686–808	0	5.507	0
781–1183	0 (align right)	9.252	808–959	0	0	0
			959–1147	0	0	0
Total	1.141	55.081	Total	1.141	55.080	2.568

[a] Corresponds to the heights of vertical layers of the EMEP model for a standard atmosphere.

A chemistry time step of 36 s in the outer nest and 12 s in the inner nest is used for chemistry in the WRF–Chem simulations. The computational demand for a one-month simulation with WRF–Chem (37 vertical layers) amounts to about 13,000 CPU hours. Each simulation started with a spin-up period of five days, from which the output is not used in the subsequent analysis. All simulations were done for July 2007.

2.3 Schemes for the OH-initiated oxidation of MEA

The degradation of MEA ($HOCH_2CH_2NH_2$) by OH has been studied extensively in the large outdoor environmental chamber European Photochemical Reactor EUPHORE (Nielsen et al., 2010; 2011; Karl et al., 2012). Major products were formamide and formaldehyde, minor products were the carbonyls 2-oxoacetamide and aminoacetaldehyde. The formation of 2-nitroaminoethanol, short MEA-nitramine, was found with yields ranging from 0.3% to 1.5%, depending on the NO_x-level in the experiment (Nielsen et al., 2011). Initial CH_2:NH_2:CH_2HO branching ratios through H-abstraction by OH radicals were reported to be 0.8:0.1:0.1 (Nielsen et al., 2010) and 0.8:0.15:0.05 (Karl et al., 2012). The higher contribution of abstraction at the $–NH_2$ group by Karl et al. (2012) takes into account that the MEA-nitramine signal by PTR-TOF-MS had not been corrected for possible generation of ionic fragments upon protonation.

In the atmosphere, reaction with hydroxyl (OH) radicals is probably the most important gas phase sink for emitted MEA, however reaction with other atmospheric oxidants like the nitrate (NO_3) radical, ozone (O_3) and the chlorine (Cl) atom may be relevant in certain geographical regions (e.g. coastal regions) and at night time (Nielsen et al., 2012). The rate coefficient for the reaction between OH and MEA, $k_{1,OH}$, has been established by three independent studies using different rate determination methods and chambers; and is in the range of $7–9 \times 10^{-11}$ cm^3 $molecule^{-1}$ s^{-1} (Borduas et al., 2013; Onel et al., 2012; Karl et al., 2012). Using the room temperature rate coefficient of 7.6×10^{-11} cm^3 $molecule^{-1}$ s^{-1} by Onel et al. (2012) and an average 12 h daytime OH concentration of 2×10^6 molecule cm^{-3} (Atkinson and Arey, 2003) the lifetime of MEA in the OH-reaction is less than 2 hours. Using the rate coefficient of 1.5×10^{-13} cm^3 $molecule^{-1}$ s^{-1}, derived with a quantitative structure property relationship (QSPR) method using molecular descriptors from semi-empirical quantum mechanics (see details in Karl et al., 2012), and an average 12 h night time NO_3 concentration of 2.5×10^8 molecule cm^{-3} (Atkinson and Arey, 2003), results in a lifetime of 7–8 hours; rendering the NO_3 reaction the most important sink of MEA at night. Recently, the rate coefficient of the reaction between O_3 and MEA was determined experimentally to be 1.09×10^{-18} cm^3 $molecule^{-1}$ s^{-1} (Borduas et al., 2013). With a 24 h average O_3 concentration of 7×10^{11} molecule cm^{-3} (~ 30 ppbv; Atkinson and Arey, 2003) the lifetime against O_3 is 15 days; the loss by O_3-reaction is therefore only relevant at high altitudes in winter time (Borduas et al., 2013). Finally, amines react extremely fast with Cl atoms, but only few experimental studies on this reaction exist (Nielsen et al., 2012). Using a global average Cl concentration of 1×10^4 atoms cm^{-3} (Wingenter et al., 1996) and an estimated rate coefficient of 4×10^{-10} cm^3 $molecule^{-1}$ s^{-1}, the lifetime of MEA against Cl atoms would be 3 days. Based on this lifetime evaluation, the reaction between OH and MEA appears to be the predominant gas phase loss reaction, hence the focus of this study is solely on the OH-initiated atmospheric oxidation of MEA.

Two different MEA oxidation schemes were included in this study: (1) a simplified scheme, referred to as MEA-Simple described in Karl et al. (2014), and (2) a more detailed scheme, referred to as MEA-Detail, developed by Karl et al. (2012) which includes the most relevant reaction paths of the OH-initiated MEA oxidation. The MEA-Detail scheme includes 17 reactions and 17 species. The MEA-Simple scheme includes only 7 reactions and species. MEA-Simple was mainly developed to predict concentrations of nitrosamines and nitramines, while formation of carbonyls was treated with less detail despite these being the major oxidation products. MEA-Detail was partly evaluated with chamber experiments in the EUPHORE (Karl et al., 2012).

The two schemes are illustrated in Fig. 2. Main features of MEA-Detail, in contrast to MEA-Simple, include: (1) the use of $k_{1,OH}$ as determined by Karl et al. (2012); (2) the use of a higher branching at the $–NH_2$-group (0.15 instead of 0.08 in MEA-Simple); (3) explicit treatment of 2-nitrosoaminoethanol ($HOCH_2CH_2N$-NO; NMEA) formation; (4) detailed treatment of the chemistry following H-abstraction at the $–CH_2$ and $–CH_2OH$ groups; and (5) formation of isocyanic acid.

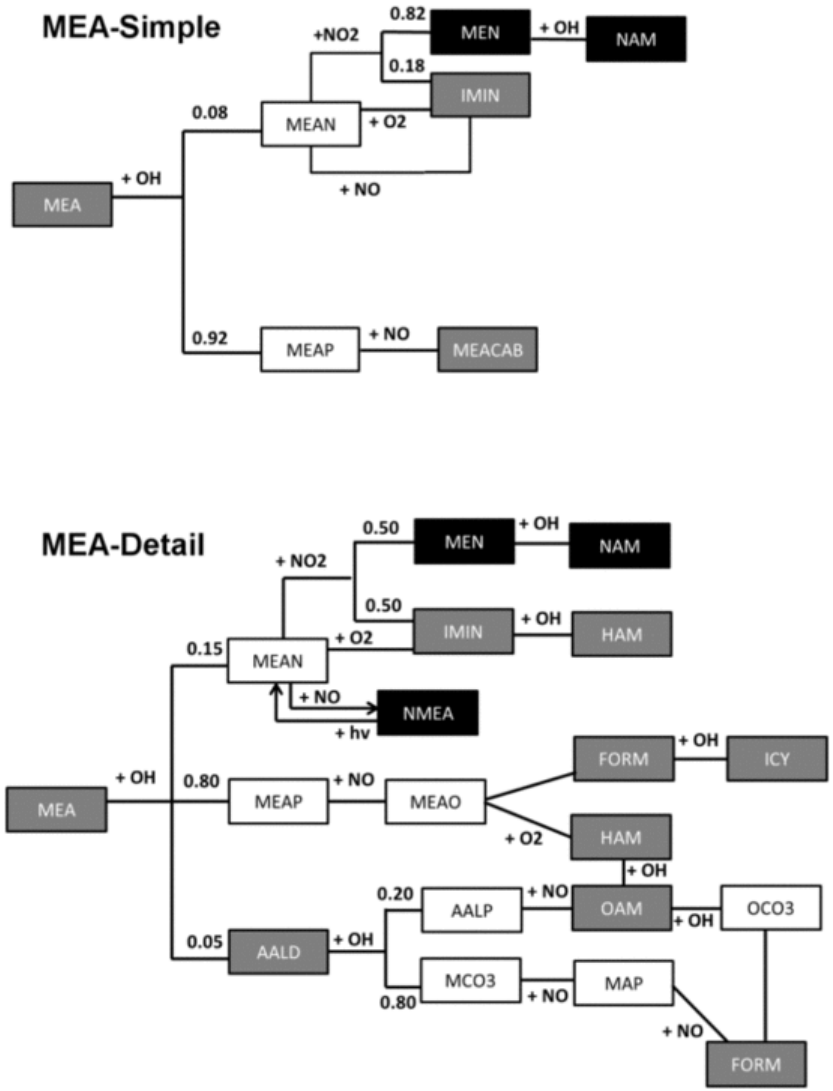

Fig. 2 Illustration of detailed and simple MEA chemistry. Black boxes indicate toxic products, grey boxes indicate other stable compounds, and white boxes indicate short-lived radicals. Important branching ratios are indicated above the respective reaction line. See explanation in the text on the differences between MEA-Simple and MEA-Detail. Identical compounds in both schemes: MEAN, N-aminoethanol radical; MEAP, peroxy radical of MEA in the first oxidation step; MEN, 2-nitroaminoethanol; IMIN, 2-iminoethanol; NAM, N-nitro hydroxyacetamide. Stable compounds that form only in MEA-Simple: MEACAB, surrogate compound representing all carbonylic products. Stable compounds that form only in MEA-Detail: NMEA, 2-nitosoaminoethanol; FORM, formamide; AALD, 2-aminoacetaldehyde; HAM, 2-hydroxyacetamide; ICY, isocyanic acid; OAM, 2-oxoacetamide.

Abstraction at the $–CH_2$ group is the major route for the OH-oxidation, producing formamide ($HCONH_2$; FORM), formaldehyde (HCHO), and 2-hydroxyacetamide ($H_2NC(=O)CH_2OH$; HAM). The latter can react further with OH to give 2-oxoacetamide ($H_2NC(=O)CHO$; OAM). FORM and OAM are also produced in the further oxidation of 2-aminoacetaldehyde. Isocyanic acid (ICY) is formed with a 100% yield in the OH-reaction of formamide, with a rate constant of 4.0×10^{-12} cm^3 $molecule^{-1}$ s^{-1} (Barnes et al., 2010).

MEA-Detail describes the first steps of OH-initiated oxidation of MEA via H-abstraction at the $–NH_2$ group as follows: 15% of the abstraction takes place at $–NH_2$ creating the N-aminoethanol radical ($HOCH_2CH_2N^*$), and subsequent reactions of the N-amino radical with NO and NO_2 lead to the corresponding nitrosamine and nitramine, respectively:

$HOCH_2CH_2NH_2 + OH \rightarrow HOCH_2CH_2N^*$ **(R1a)**

$HOCH_2CH_2N^* + NO \rightarrow HOCH_2CH_2N\text{-}NO$ **(R2)**

$HOCH_2CH_2N^* + NO_2 \rightarrow HOCH_2CH_2N\text{-}NO_2$ **(R3a)**

$HOCH_2CH_2N^* + NO_2 \rightarrow HONO + HOCH_2CH = NH$ **(R3b)**

$HOCH_2CH_2N^* + O_2 \rightarrow HOCH2CH = NH$ **(R4)**

The ratio $[NO]/[NO_2]$ determines the competition between formation of 2-nitosoaminoethanol (MEA-nitrosamine, $HOCH_2CH_2N$-NO; NMEA) through (R2) or 2-nitroaminoethanol (MEA-nitramine; $HOCH_2CH_2N$-NO_2; MEN) through (R3a). The rate constant for (R2) used in MEA-Detail was estimated based on the consideration that MEA-nitrosamine will not form in significant amounts under ambient atmospheric NO levels. At a typical atmospheric $[NO]/[NO_2]$ of 0.25, the ratio between the reaction rates of (R2) and (R3) is only 0.15. However, at high NO levels close to the source, the formation of MEA-nitrosamine could become significant. At daylight nitrosamines are rapidly destroyed by photolysis. In MEA-Detail, photolysis of the MEA-nitrosamine is taken into account (Karl et al., 2012), recycling the N-amino radical:

$HOCH_2CH_2N\text{-}NO + h\nu \rightarrow HOCH_2CH_2N^* + NO$ **(R5)**

Karl et al. (2012) assumed that the MEA-nitrosamine, despite forming in reaction (R2), quickly undergoes photolysis, which would explain why it was not detected in any of the experiments (Karl et al., 2012; Nielsen, 2011).

In MEA-Simple the formation of a nitrosamine in the oxidation of MEA was deactivated. Instead, the reaction between NO and the N-amino radical leads directly to the imine. Recent quantum chemical calculations provided evidence that nitrosamine from primary amines, despite they could form under atmospheric conditions, is in isomerization equilibrium with $RNHNOH^+$ which undergoes rapid H-abstraction by O_2 to give the corresponding imine within seconds (Tang et al., 2012). Imines were postulated to be relevant gas-phase products in the photo-oxidation of amines, however literature reports on imines are scarce (Nielsen et al., 2012). In the case of MEA, the corresponding imine is 2-iminoethanol ($HOCH_2CHNH$; IMIN). In recent MEA photo-oxidation experiments, Borduas et al. (2013) detected a signal by online chemical ionization mass spectrometry (CI-TOFMS) that could be associated with 2-iminoethanol. However, 2-aminoacetaldehyde (H_2NCH_2CHO; AALD), which forms upon H-abstraction at $–CH_2OH$ group has the same mass to charge ratio in the CI-TOFMS.

Further differences between MEA-Simple and MEA-Detail with respect to the formation of MEA-nitramine are detailed in Table 4. Using a NO_x mixing ratio of 4.0 ppbv and $[NO]/[NO_2]$ of 0.25 as typical conditions in the area of Mongstad, the rate k_{3a}·$[NO_2]$ for the reaction of the N-amino radical to give MEA-nitramine in MEA-Detail is four times smaller than in MEA-Simple. MEA-Simple uses rate constant $k_{3a} = 3.20 \times 10^{-13}$ cm^3 $molecule^{-1}$ s^{-1} as determined by Lazarou et al. (1994) for the reaction of the dimethyl amino radical with NO_2. MEA-Detail uses rate constant $k_{3a} = 7.0 \times 10^{-14}$ cm^3 $molecule^{-1}$ s^{-1} as reported by Nielsen et al. (2010). The latter was included in the gas-phase reaction scheme for MEA that was evaluated in chamber experiments (Karl et al., 2012); however concentrations of MEA-nitramine measured by PTR-MS were associated with an uncertainty of a factor of 3.

Table 4 Differences in the kinetic parameters in the branching at the $–NH_2$ group of MEA. Assuming typical mixing ratios: $[NO_X]$ = 4.0 ppbv, $[NO]/[NO_2]$ = 0.25, $[O_2]$ = 78%.

Parameter p	MEA-sSimple	MEA-dDetail	Ratio p(MEA-Detail)/p(MEA-Simple)
k_{1a}	0.61 × 10^{-11} cm^3 $molecule^{-1}$ s^{-1}	1.38 × 10^{-11} cm^3 $molecule^{-1}$ s^{-1}	2.27
k_2*[NO]	0.0016 s^{-1}	0.0017 s^{-1}[a]	1.01
k_{3a}*$[NO_2]$	0.0252 s^{-1}	0.0055 s^{-1}	0.22
k_{3b}*$[NO_2]$	0.0055 s^{-1}	0.0055 s^{-1}	0.99
k_4*$[O_2]$	2.40 s^{-1}	2.30 s^{-1}	0.96
$\frac{k_{3a}[NO_2]}{k_2[NO]+k_3[NO_2]+k_4[O_2]}$	0.0104	0.0024	0.23
$\frac{k_4[O_2]+k_{3b}[NO_2]}{k_2[NO]+k_3[NO_2]+k_4[O_2]}$	0.989	0.997	1.01

[a] Max value of the net reaction in the dark (photolysis of nitrosamine during daytime gives a lower net reaction rate).

Nitramines are thought to be photo chemically stable compounds with long atmospheric lifetime (Grosjean, 1991). A SAR estimate for the rate constant of OH radicals with MEA-nitramine however indicates a shorter lifetime for this nitramine, i.e.

~ 0.5 days. Both MEA schemes allow for reaction between MEA-nitramine and OH radicals to form N-nitro hydroxyacetamide ($HOCH_2C(=O)N\text{-}NO_2$; NAM) with a rate constant of 1.48×10^{-11} cm^3 $molecule^{-1}$ s^{-1} (Karl et al., 2012).

The RACM mechanism in WRF–Chem was extended to include the two schemes MEA-Simple and MEA-Detail by using the Kinetic Pre Processor (KPP). KPP automatically generates Fortran codes needed to perform the integration of chemical equations for the new species. Additionally, the necessary terms to account for treatment of the various parameterized physical processes (emissions, deposition, photolysis, initializations, etc.) were added for all new species in the respective subroutines of WRF–Chem. Time-dependent atmospheric concentrations of OH, NO, and NO_2 and zenith angle will be influential in determining the production of the nitrosamine and nitramine from emitted MEA.

3 Results

3.1 Evaluation of WRF–Chem

A detailed evaluation of the WRF model using ECMWF reanalysis meteorological data for ICs and BCs including five local weather monitoring stations (Bergen, Fedje, Flesland, Takle, and Kvamskogen) in the region of Bergen has been performed in the study by Karl et al. (2014), and satisfactory agreement with the observed hourly data on 2 m-temperature and frequencies of wind direction and wind speed was found. The WRF model reproduced the west–east gradient of the annual precipitation amount, which is due to the orographic rainfall when humid Atlantic air masses meet the hill chain in about 20 km distance to the east of Mongstad. However, the average precipitation amount, and the rainfall frequency in July over the flat terrain in the coastal area around Mongstad, is underestimated by WRF. A limited evaluation of the meteorological performance of the WRF–Chem model was made for temperature, wind speed and wind direction with observations from 6 weather stations in the region. Table S1 (in the Supplementary materials) summarizes the statistics of the evaluation in the form of monthly mean (modelled, observed), overall bias (mean difference), root-mean-square error (RMSE) and correlation.

Very good correlation between model and observation was found for 2 m-temperature. For instance at Takle, 30 km northeast from Mongstad, overall bias, RMSE and correlation were 0.7 °C, 1.1 °C, and 0.94, respectively. Good correlation between model and observation was found for 10 m-wind speed at all stations. For instance at Fedje, located on an island 17 km west from Mongstad, the overall bias, RMSE and correlation were – 1.1 m s^{-1}, 2.3 m s^{-1} and 0.81. At Fedje, frequently very high wind speeds are observed. The observed monthly mean wind speed in July 2007 was 5 m s^{-1}. For the other stations, WRF–Chem slightly overestimated wind speed, with absolute bias in the range of 0.1–1.4 m s^{-1}.

While the correlation between modelled and observed monthly mean wind direction was still acceptable, quite large discrepancies of the mean wind direction were obvious for Modalen, Kvamskogen, Bergen-Flesland, and Bergen-Airport. Difficulties in predicting wind direction might arise from the complex terrain at the west coast of Norway, due to local mountain wind systems and sea-breeze systems. For instance, at Bergen-Flesland mean wind direction predicted by WRF–Chem is SSE, while observed mean wind direction is WNW. For the stations closer to Mongstad (Fedje and Takle), the absolute agreement with observed wind direction appears to be better.

The performance of WRF–Chem for calculating the variability of air pollutants (O_3, NO, and NO_2) during July 2007 was evaluated at the measurement site Hamna [60°48′00″ N; 5°03′43″ E; 9 m a.s.l.], located 3 km downwind of Mongstad. Included in the evaluation were the baseline configurations of both WRF–EMEP and WRF–Chem (simulation Base), and the WRF–Chem simulations HiVert (high vertical resolution) and DetailMEA (high vertical resolution and detailed MEA oxidation). Table 5 provides an overview of the computed monthly mean concentration, overall bias, RMSE, and correlation for the four model simulations. Since the concentrations from the corresponding model grid point (with cell size 2 × 2 km^2) are not necessarily representative for the point of observation, the weighted mean of the surrounding eight grid points was used in the evaluation.

Table 5 Evaluation of WRF-Chem model with hourly air quality observation data at Hamna [60°48′00″ N; 5°03′43″ E; 9 m a.s.l.], in July 2007: monthly mean (ppbv), overall absolute bias (ppbv) and percentage bias in brackets, RMSE (ppbv), correlation (Pearson r). Model values are weighted averages of the corresponding model grid point and the eight surrounding grid points. Observed means are: 29.2 ppbv O_3, 1.38 ppbv NO, and 31.9 ppbv O_X.

Compound	Evaluation parameter	WRF–EMEP	WRF-Chem		
		Base	Base	HiVert	DetailMEA
O_3	Mean	26.6	33.7	32.4	32.3
	Bias	– 2.70 (– 9.2%)	4.45 (15%)	3.10 (11%)	3.13 (11%)
	RMSE	8.35	9.12	8.37	8.37
	Correlation	0.26	0.50	0.50	0.50
NO	Mean	0.754	0.152	0.146	0.146
	Bias	– 0.63 (– 46%)	– 1.24 (– 89%)	– 1.24 (– 90%)	– 1.24 (– 89%)
	RMSE	2.63	2.60	2.61	2.61
	Correlation	0.08	0.30	0.29	0.29

$O_x(O_3 + NO_2)$	Mean	28.9	35.1	33.8	33.8
	Bias	– 3.12 (– 9.7%)	3.12 (9.8%)	1.82 (5.7%)	1.81 (5.7%)
	RMSE	7.98	7.78	7.08	7.08
	Correlation	0.26	0.58	0.59	0.59

Observed monthly mean O_3 concentration was slightly underestimated by the Base simulation with the WRF–EMEP model (overall bias – 2.70 ppbv) and overestimated by all WRF–Chem simulations (range of overall bias: 3.10–4.45 ppbv). For the Base configuration of WRF–Chem, the overall bias, RMSE and correlation were 4.45 ppbv, 9.12 ppbv and 0.50. Correlation for O_3 concentration in the WRF–Chem simulations was 0.50 (see Fig. 3B). The correlation of the WRF–EMEP Base simulation was weaker (0.26) which was probably related to a period with elevated O_3 concentrations (40–60 ppbv) in the period 5–7 July during which WRF–EMEP underestimated observed O_3 by 20–40 ppbv (Fig. 3A). The ozone episode was well captured by the WRF–Chem Base simulation. The ozone episode coincided with plume passages at Hamna in both models (indicated by modelled MEA peak concentrations). According to the models, the ozone episode was characterized by low boundary layer height (< 300 m) and by enhanced photochemical production of MEA-nitramine in ground-level air. Note that WRF–Chem uses initial and boundary conditions for O_3 from Oslo CTM2 every 6 h, whereas WRF–EMEP uses climatological O_3 values as boundaries to the outer domain (50-km resolution). The time series of hourly averaged O_3 reveals that WRF–Chem Base occasionally overestimated observed O_3 between 23 and 26 July but overall matched well the daily variation and magnitude of O_3 during July (Fig. 3A).

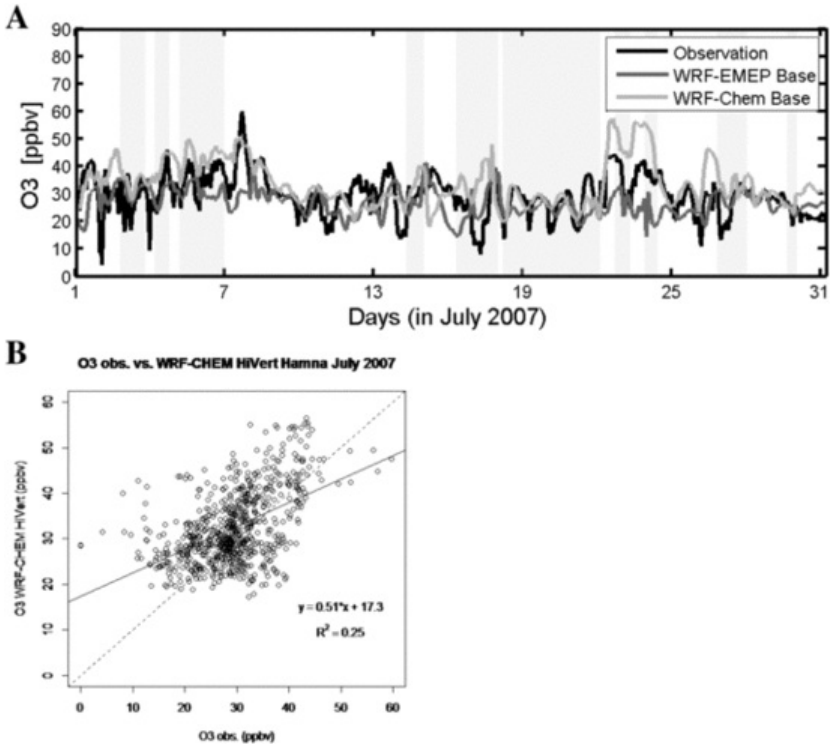

Fig. 3 Evaluation of ozone mixing ratios in the ground-level air at Hamna: (A) Time series of hourly averaged O_3 mixing ratios from observations at Hamna (black line), as well as grid-averaged modelled surface O_3 concentrations from WRF–EMEP (dark grey line) and WRF-Chem (light grey line) Base simulations (both have 20 vertical layers); and (B) Correlation of hourly averaged O_3 air mixing ratios (in ppbv) from observations at Hamna and grid-averaged modelled surface O_3 concentration with WRF-Chem simulation Base. The 1:1 line is indicated as dashed line and the regression line as black line. Grid-averaged model values are a weighted average of the corresponding model grid point and the eight surrounding grid points. Days with plume passage at Hamna (indicated by modelled MEA concentration peaks > 50 ng m^{-3}) are marked with greyish background in figure part (A).

Observed monthly mean NO concentration is underestimated by the models, with an overall bias of about – 50% and – 90% in WRF–EMEP and WRF–Chem, respectively. The underestimation might be due to the dilution of the NO emissions from Mongstad (from the power plant equipped with PCCP and the refinery) by treating the point source as a volume source in the models, or due to an underestimation of the NO emissions from the refinery area. For the Base configuration of WRF–Chem, the overall bias, RMSE and correlation of the modelled NO concentration were – 1.24 ppbv, 2.60 ppbv and 0.30. Emitted NO from the power plant equipped with PCCP and the refinery at Mongstad reacts immediately with O_3 to form NO_2 and O_2. Due to this titration effect, it

is more robust to compare O_x (i.e., the sum of O_3 and NO_2) concentrations than NO_2 alone. Good correlation was found for O_x concentrations in the WRF-Chem simulations, indicating that WRF-Chem quite well captures the fast photochemical conversion in the vicinity of the refinery area.

WRF-Chem was further evaluated for its capability of predicting the integrated NO_2 concentrations from ground-level to the top of the troposphere. Tropospheric columns of NO_2 are mostly influenced by surface emissions and processes in the lower troposphere. Tropospheric columns of NO_2 retrieved from OMI satellite data was used to evaluate the computed NO_2 columns over the inner domain of WRF-Chem simulation HiVert (37 vertical layers). The uncertainty of the column values in the pixels derived from OMI satellite is rather large; the error of the observations is 30% or higher. Further, the resolution of the modelled column values is higher, 10 × 10 km^2 (taken from the coarse domain), limiting the comparability of model and satellite data. With this in mind, the match between observed and modelled spatial distribution of the tropospheric columns of NO_2 is surprisingly good (Figure S1A and S1B in the Supplementary materials). OMI data shows highest NO_2 column in the city of Bergen (about 2.0 × 10^{15} molecules cm^{-2}), where the model data shows a much lower value (about 1.3 × 10^{15} molecules cm^{-2}), which could indicate missing NO_x emissions from the city of Bergen in the TNO-MACC emission database. For the satellite pixel containing Mongstad, the agreement between observation and model is rather good, both on the monthly average and for the time series in July 2007 (Figure S1C), when taking into account the different spatial resolution.

3.2 Comparison between WRF-Chem and WRF-EMEP

All simulations with the WRF-EMEP and the WRF-Chem model included a chemically inert tracer compound TMEA emitted with the same amount as MEA and with the same deposition properties but not reacting with OH radicals. Table 6 provides an overview of the results from the different model simulations. Monthly mean (July 2007) ground-level air concentration of TMEA inside the 40 × 40 km^2 study area grid with the capture plant in the centre agrees fairly well between WRF-EMEP and WRF-Chem Base run, both using 20 vertical layers. The grid maximum of monthly mean TMEA in the study grid is located close to the PCCP emission source and is found to be 176.1 ng m^{-3} and 177.8 ng m^{-3} in WRF-EMEP Base and WRF-Chem Base, respectively. The grid average of monthly mean TMEA in WRF-Chem Base was 16% higher than in WRF-EMEP Base which indicates less effective deposition in WRF-Chem. The three WRF-Chem scenario simulations that use 37 vertical layers (HiVert, DetailMEA, and NoRefNOx) resulted in identical monthly mean concentrations of TMEA; with a spatial maximum of 199.4 ng m^{-3} and spatial average of 4.0 ng m^{-3}.

Table 6 Comparison of modelled monthly mean ground-level air concentration of MEA and related oxidation products as well as deposition rates of MEA in the 40 km × 40 km study area for July 2007. Simulations considered dry and wet deposition of MEA and related oxidation products. Given values of air concentrations and deposition fluxes are the maximum in the study grid, and in brackets the grid-average. Ground-level air concentration refers to the concentration in the lowest model layer.

	WRF-EMEP Base	WRF-Chem Base	WRF-Chem HiVert	WRF-Chem DetailMEA	WRF-Chem NoRefNOx
Ground-level air concentration TMEA, inert tracer (ng m^{-3})	176.1	177.8	199.4	199.4	199.4
	(4.4)	(5.1)	(4.0)	(4.0)	(4.0)
Ground-level air concentration MEA (ng m^{-3})	175.1	164.4	187.8	186.9	185.6
	(4.2)	(3.4)	(2.8)	(2.6)	(2.4)
Ground-level reacted MEA (ng m^{-3})	1.7	13.4	11.9	12.8	14.0
	(0.2)	(1.7)	(1.3)	(1.4)	(1.6)
Ground-level air concentration MEA-nitramine (pg m^{-3})	13.6	8.5	6.2	2.8	3.5
	(1.4)	(1.4)	(1.1)	(0.5)	(0.3)
Ground-level air concentration MEA-nitrosamine (pg m^{-3})	–	–	–	0.3	0.4
				(0.01)	(0.01)
Total deposition flux MEA (mg m^{-2})	5.55	5.14	5.30	5.29	5.29
	(0.11)	(0.15)	(0.14)	(0.14)	(0.14)
Wet deposition flux MEA (mg m^{-2})	2.27	4.61	4.57	4.57	4.57

	(0.05)	(0.12)	(0.12)	(0.12)	(0.12)
Dry deposition flux MEA at location of max. tot. dep. (mg m^{-2})	3.28	0.53	0.73	0.73 (align left)	0.73
	(0.06)	(0.03)	(0.02)	(0.02)	(0.02)

Monthly mean air concentration of MEA inside the 40 × 40 km^2 study area varied between 164 and 188 ng m^{-3} as grid maximum (close to the PCCP) and between 2.4 and 4.2 ng m^{-3} as grid average. The spatial distribution of monthly mean MEA concentration at ground-level resulted from WRF-Chem Base showed a wider impact area of MEA than the WRF-EMEP Base simulation (Fig. 4B), with MEA concentrations of > 10 ng m^{-3} within a radius of ca. 10 km around Mongstad. The much smaller extent of the impacted area in WRF-EMEP Base is likely due to more effective deposition of MEA in the vicinity of Mongstad. In the WRF-Chem Base simulation, total deposition flux of MEA was 8% lower and dry deposition flux of MEA was four times lower at the grid maximum than in WRF-EMEP Base (see Table 6). An explanation for the more efficient dry deposition of MEA in WRF-EMEP Base is the consideration of co-deposition effects in the dry deposition parameterization of the EMEP model. The effect of dry and wet deposition in WRF-EMEP Base has been tested in separate runs. It was found that dry deposition reduced the grid maximum of MEA by ~ 40% compared to a run without deposition, while wet deposition had a negligible effect on the grid maximum of MEA.

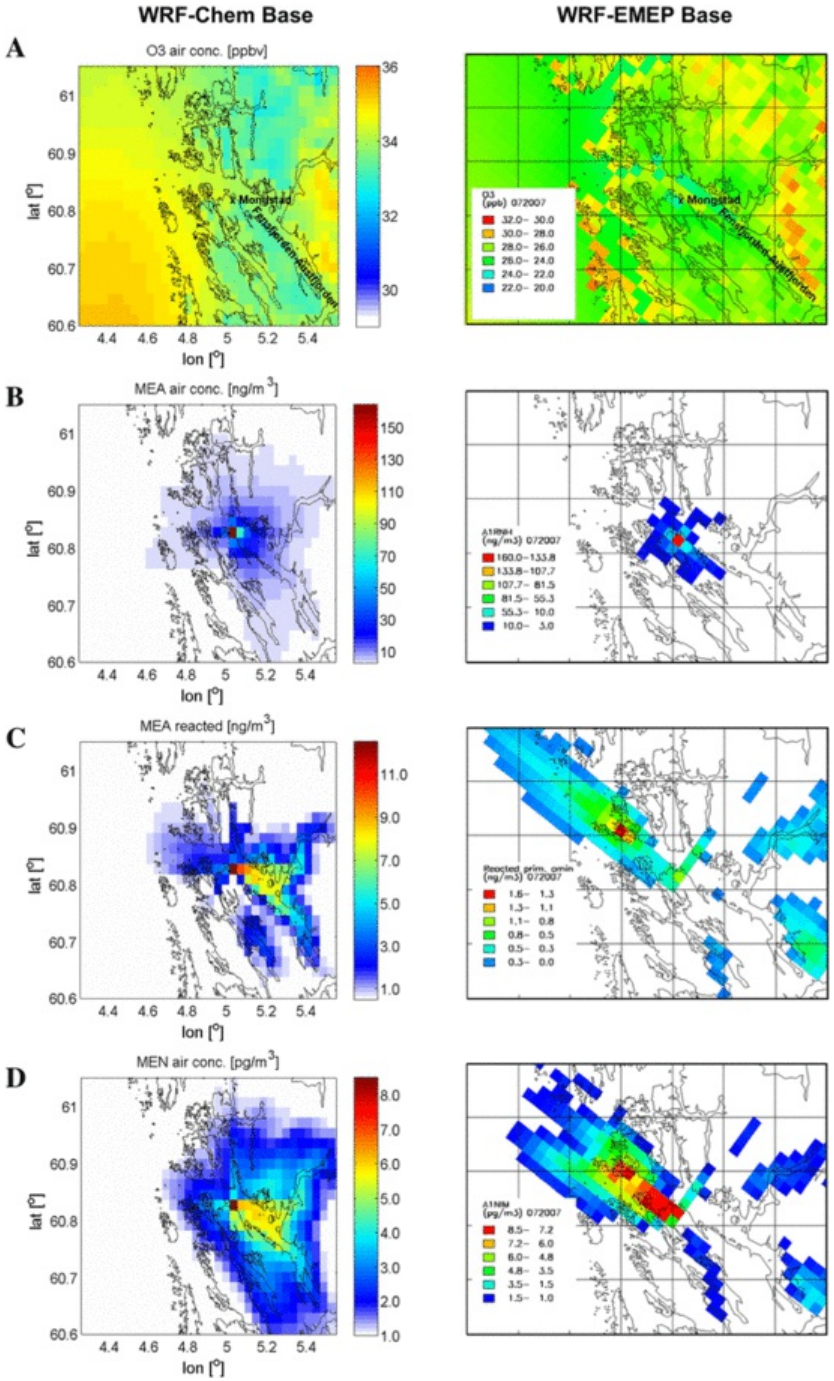

Fig. 4 Comparison of WRF-Chem Base (left) to WRF-EMEP Base (right) ground-level air concentrations in the 40 × 40 km^2 study region: (A) monthly mean O_3 mixing ratio (ppbv), (B) monthly mean MEA concentration (ng m^{-3}), (C) monthly mean reacted MEA (ng m^{-3}), and (D) monthly mean

MEA-nitramine air concentration (pg m^{-3}).

On spatial average, ground-level air concentration of MEA in WRF-Chem Base was 19% lower than in WRF-EMEP Base because the reaction of MEA with OH radicals is much more important in WRF-Chem. Reacted MEA, which was calculated as the difference of the ground-level concentrations of unreactive TMEA and MEA, was 8 times higher in WRF-Chem Base than in WRF-EMEP Base, both for the respective grid maximum and on grid average. In WRF-Chem the location of maximum reactivity was close to the source (Mongstad) while in WRF-EMEP it was ca. 14 km northwest of the PCCP (Fig. 4C). The higher reaction rate of MEA + OH is expected to result in higher simulated concentrations of the oxidation products of MEA, such as MEA-nitramine. Indeed, the spatial distribution of MEA-nitramine in the study grid is related to the spatial distribution of reacted MEA in the respective WRF-Chem Base and WRF-EMEP Base simulation (Fig. 4C and D).

Monthly mean MEA-nitramine concentrations have similar grid maximum and grid average values in the two simulations (Table 6) despite much higher reacted MEA in WRF-Chem Base. Since both simulations employ the MEA-Simple chemistry scheme, limited availability of NO_2 in WRF-Chem is the only possible reason for similar MEA-nitramine concentrations. Monthly mean NO_x in ground-level air in the in the area around Mongstad and in Fensfjorden–Austfjorden modelled by WRF-Chem Base were in the range of 0.8–1.9 ppbv, about 2–3 times lower than in WRF-EMEP Base (2.0–4.5 ppbv). Monthly mean modelled NO_2 mixing ratio at the monitoring site Hamna (3 km downwind of Mongstad) was 1.39 ppbv and 2.03 ppbv in WRF-Chem Base and WRF-EMEP Base, respectively. One reason for the higher reactivity in the WRF-Chem Base simulation were the higher modelled monthly mean mixing ratios of O_3 (Fig. 4D) in the area around Mongstad (32–34 ppbv) compared to the WRF-EMEP Base simulation (24–28 ppbv). At Hamna, modelled hourly average O_3 was frequently higher in WRF-Chem than in WRF-EMEP (Fig. 3A).

Fig. 5 displays the modelled time series of MEA and OH (hourly averages) at the monitoring station Hamna from the different simulations using WRF-EMEP and WRF-Chem. Modelled monthly mean concentrations of MEA at Hamna (ground-level) were 14.3 ng m^{-3} and 19.1 ng m^{-3} in the WRF-EMEP Base and WRF-Chem Base simulations, respectively. O_3 is the main photochemical precursor of OH radicals in the simulations. However, OH recycling is influenced by NO_x levels and by presence of volatile organic compounds. The influence of OH on the reactivity of MEA at Hamna (ground-level) can be investigated by comparing days with and without plume passage. Modelled hourly MEA peaks with concentration > 50 ng m^{-3} was used as indication for passage of the PCCP plume at Hamna (indicated as yellow bars in Fig. 5). Common plume passage in WRF-Chem and WRF-EMEP during daytime were detected on 4, 5, and 16 July. On days without plume passage at Hamna, for example from 8–13 July, modelled maximum daytime OH in WRF-Chem Base was a factor of 2–4 lower than in WRF-EMEP Base. On days with common plume passage, modelled maximum daytime OH in WRF-Chem Base was higher or similar high as in WRF-EMEP Base. To conclude about the reactivity of MEA in the two simulations, only hours with plume passage at Hamna were considered. The average modelled OH concentration during plume passage was 1.88 × 10^6 cm^{-3} and 1.47 × 10^6 cm^{-3} in WRF-Chem Base and WRF-EMEP Base, respectively.

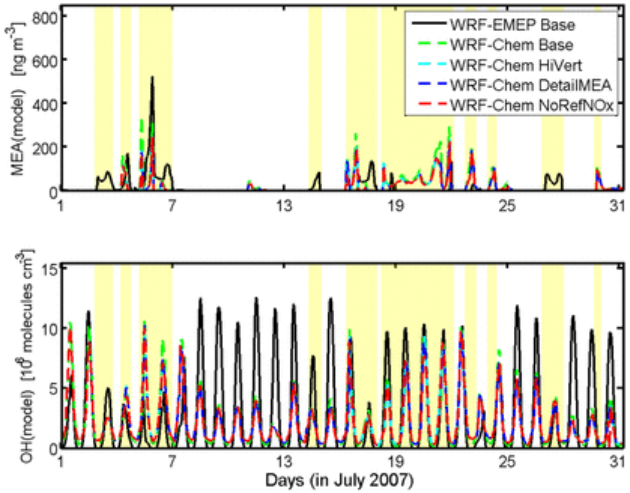

Fig. 5 Modelled air concentration time series of MEA and OH at Hamna at ground-level for days in July 2007: modelled hourly MEA concentration (top panel) and modelled hourly OH concentration (bottom panel). Results from all simulations included: WRF-EMEP Base (solid black line), WRF-Chem Base (green dashed line), WRF-Chem HiVert (cyan dashed line), WRF-Chem DetailMEA (dark blue dashed line), and WRF-Chem NoRefNOx (red dashed line). Days with modelled MEA concentration peaks > 50 ng m^{-3}, indicating plume passage at Hamna, are marked with yellow background. (For interpretation of the references to colour in this figure legend, the reader is referred to the web version of this article.) (Figure 5 should be color in print as well, therefore the statement about the color references can be deleted.)

Modelled monthly average concentrations of OH at Hamna were 2.16 × 10^6 molecules cm^{-3} and 2.67 × 10^6 molecules cm^{-3} in the WRF-Chem Base and WRF-EMEP Base simulations, respectively. However, days when modelled OH was higher in WRF-EMEP Base were without plume passage (see example above) and therefore not relevant for determining the reactivity of MEA. On the other hand, WRF-Chem predicted higher OH concentration during night, which influences reactivity of MEA in the study grid because MEA emissions from the PCCP occurred day and night. Minimum OH at night was 1–2 × 10^5 cm^{-3} in WRF-Chem Base while it was close to zero (< 10^4 cm^{-3}) in WRF-EMEP Base. When using higher vertical resolution (WRF-Chem HiVert), OH

did not fall below 2.6 × 10^5 cm^{-3} at night. Reaction of alkenes with O_3 is a source of OH at night which is included in the regional atmospheric chemistry scheme RACM used in the WRF-Chem simulations. EMEP chemistry includes OH formation from reactions isoprene + O_3 and propene + O_3 but not from the reaction of monoterpenes with O_3.

The atmospheric MEA mass balance in the 200 × 200 km^2 inner domain from WRF-Chem Base and WRF-EMEP Base simulations was inspected (Table S2). In WRF-Chem Base reaction of MEA with OH radicals was the major loss pathway; about 44% (i.e. ~ 1500 kg) of the emitted MEA amount (~ 3400 kg) underwent reaction with OH radicals. The corresponding reactive loss of MEA was only 17% in WRF-EMEP. Wet deposition was the second most important loss in WRF-Chem Base (~ 1060 kg) while dry deposition was a minor loss (~ 250 kg). Total deposition was similar as in WRF-EMEP Base. Net transport of MEA out of the inner domain was responsible for 17% of MEA loss (i.e. ~ 570 kg), much less than in WRF-EMEP Base (41% or ~ 1400 kg). In conclusion, reactivity of MEA in WRF-Chem was almost three times higher than in WRF-EMEP, reducing the amount of MEA that was transported out of the inner domain.

3.3 Effect of vertical resolution

The vertical resolution in WRF-Chem was increased in simulation HiVert using 37 vertical model layers compared to 20 vertical layers in simulation Base. Modelled vertical profiles of TMEA concentration, reacted MEA, and OH concentration at Hamna from simulations WRF-Chem Base and HiVert are presented in Fig. 6.

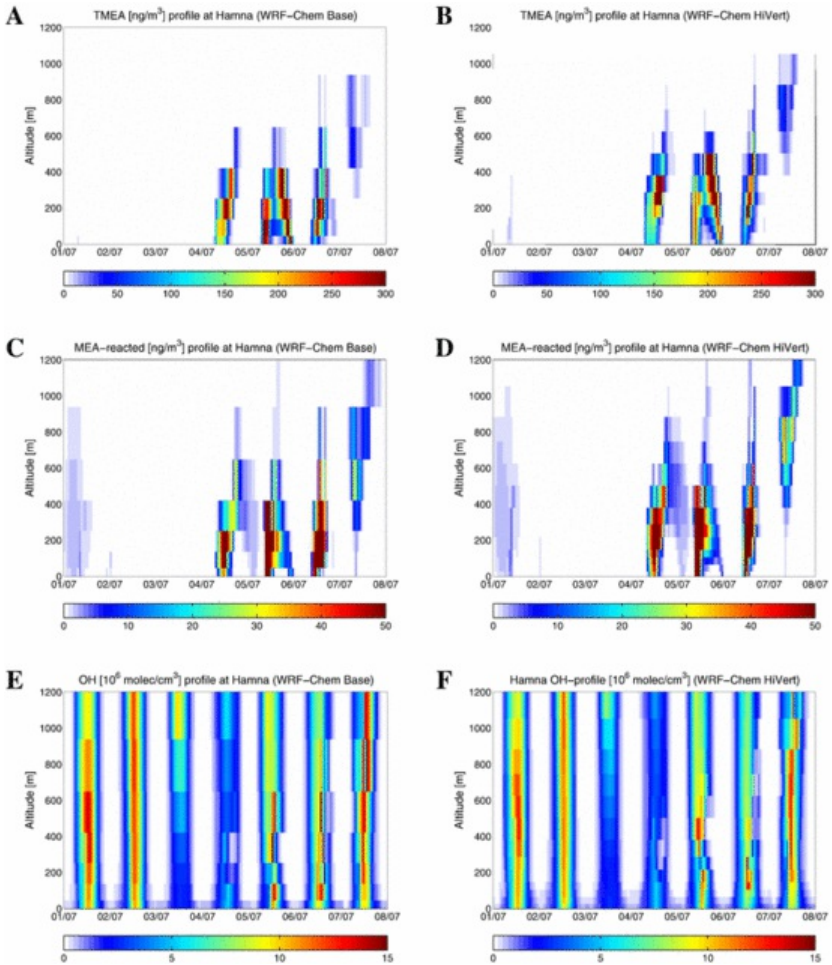

Fig. 6 Vertical profiles of modelled concentrations at Hamna (up to 1200 m altitude) from 1–8 July 2007 from simulation WRF-Chem Base (left) using 20 vertical layers and WRF-Chem HiVert (right) using 37 vertical layers: (A) TMEA concentration (ng m^{-3}) WRF-Chem Base, (B) TMEA concentration WRF-Chem HiVert, (C) MEA reacted (ng m^{-3}) WRF-Chem Base, (D) MEA reacted WRF-Chem HiVert, (E) OH radical concentration (10^6 cm^{-3}) WRF-Chem Base, and (F) OH radical concentration WRF-Chem HiVert.

Plume passage at Hamna in the beginning of July 2007 (1–8 July) was found on three days, 4–6 July, with plume height from ground to 600 m. Plume passage was also found on 7 July, at an altitude of 400–1000 m. Modelled TMEA concentrations in simulation HiVert at an altitude of 300–600 m were higher than in simulation Base (Fig. 6A and B); especially at 400–500 m height TMEA concentrations in simulation HiVert were up to ca. 200 ng m^{-3} higher than in simulation Base.

Differences between modelled MEA concentrations in simulations Base and HiVert might be a result of: (1) different vertical attribution of MEA emissions from the PCCP (Table 3); (2) changed vertical mixing; (3) changes in the vertical resolution of the meteorology (horizontal winds); and (4) changed OH radical concentration (due to changed vertical resolution). Modelled TMEA concentrations are not affected by changes of OH, therefore only the first three reasons can explain the discrepancy. Based on the layer-specific MEA emissions given in Table 3, different vertical ~~attribution was~~ attributions were analysed. In simulation HiVert, MEA emissions below ~ 320 m height were 18% higher than in simulation Base and MEA emissions above ~ 320 m height were 33% lower than in simulation Base. Maximum MEA emission height was 564 m and 522 m in simulations HiVert and Base, respectively. Differences in the vertical attribution of MEA emissions are thus not sufficient to explain the much higher concentrations of TMEA (and MEA) at 400–500 m height in simulation HiVert. Due to lower emissions in the height range 400–500 m in simulation HiVert, TMEA concentrations were actually expected to be lower than in simulation Base. Another explanation could be different direction of horizontal wind in the two simulations. Due to higher vertical resolution, horizontal winds were better resolved in simulation HiVert and also the change of wind direction with increasing altitude. Direction of horizontal wind on 5 July (plume passage day) turned by about 180° above a height of 324 m in simulation Base (Figure S2). The corresponding wind turn in simulation HiVert was above 440 m which might explain the higher concentrations of TMEA at 400–500 m height. As a consequence, also the reactivity of MEA above 400 m height was higher in simulation HiVert (Fig. 6C and D), leading to higher concentrations of MEA-nitramine (by up to 70 pg m^{-3}) than in simulation Base. On grid-average reacted MEA and MEA-nitramine at ground-level in simulation HiVert were 24% and 21%, respectively, lower than in simulation Base (Table 6), probably due to stronger vertical mixing. Vertical OH profiles were quite similar on the plume passage days, but close to the ground (below 100 m) OH in simulation HiVert was lower by several 10^6 cm^{-3} (Fig. 6E and F). A notable OH depletion event (OH < 1 × ~~×~~10^6 cm^{-3}) coinciding with the plume passage on 4 July during daytime, occurred at 300–400 m height in both simulations, probably due to high NO_2 in the plume, demonstrating the effect of the PCCP plume on the local background air chemistry.

3.4 Simplified versus detailed MEA oxidation scheme

Differences in the computed 3-dimensional spatial distribution of MEA-related oxidation products due to the use of either the simplified reaction scheme for MEA oxidation (i.e. MEA-Simple) or the comprehensive reaction scheme (i.e. MEA-Detail) were revealed by comparison of the two WRF-Chem simulations HiVert (uses MEA-Simple) and DetailMEA (uses MEA-Detail). Oxidation products forming upon H-abstraction from the $–NH_2$ group include MEA-nitramine, MEA-nitrosamine, iminoethanol, and N-nitro hydroxyacetamide. Maximum and grid-average ground-level concentrations of MEA-nitramine (monthly mean) in the 40 × 40 km^2 study area from simulation HiVert are about twice as high as from simulation DetailMEA (see Table 7). Although the possible formation of MEA-nitrosamine is considered in MEA-Detail, maximum concentration of MEA-nitrosamine is only 0.3 pg m^{-3}, about 9 times smaller than the corresponding maximum concentration of MEA-nitramine (2.8 pg m^{-3}). On the other hand, grid maximum and average concentrations of iminoethanol from simulation HiVert are only half of the concentrations from simulation DetailMEA.

Table 7 Comparison of maximum and grid-averaged monthly mean air concentration (in ng m^{-3}) in the 40 km × ~~×~~40 km study area for July 2007 between simple MEA chemistry (simulation HiVert) and detailed MEA chemistry (simulation DetailMEA).

0.157

Compound	WRF-Chem HiVert		WRF-Chem DetailMEA	
	Grid max.	Grid average	Grid max.	Grid average
MEA-nitramine	0.0062	0.0011	0.0028	0.0005
MEA-nitrosamine		0.0003	0.00001	
N-nitro hydroxyacetamide	0.0014	0.0005	0.0006	0.0002
Iminoethanol	0.667	0.126	1.344	0.248
Sum carbonyls[a]	10.58	2.003	10.99	1.854
Formamide		~~7.488~~	7.488~~1.294~~	~~0.157~~1.294
Isocyanic acid (HCNO)		~~0.364~~	0.364~~0.157~~	0.157

[a] Sum of AALD, HAM, OAM, formamide.

The sum of carbonylic products forming in the atmospheric oxidation of MEA has similar concentrations in both simulations. Grid average concentration of the sum of carbonyls is about 2 ng m^{-3}; three orders of magnitude larger than the concentration of the sum of nitrosamines and nitramines. According to simulation DetailMEA, formamide contributes 70% to the sum of carbonyls, in line with experimental findings that formamide is the main product from atmospheric MEA oxidation. Isocyanic acid is only

identified as oxidation product in the MEA-Detail scheme. Simulation DetailMEA shows that the grid maximum concentration of isocyanic acid is only 3% of the sum of carbonyls, while the grid average concentration is 8% of the sum of carbonyls, indicative for the regional-scale production of this compound.

The distribution of oxidation products in terms of monthly average concentrations was inspected at Mongstad, Bergen (city), Modalen and Takle (Fig. 7). Bergen is 46 km south, Modalen is 47 km east, and Takle is 30 km northeast from Mongstad. MEA-nitrosamine is only found at Mongstad (0.3 pg m^{-3}), and not present at the other sites (less than 0.04 pg m^{-3}). MEA-nitramine is reduced by a factor of 7 in Bergen and Takle, compared to Mongstad. Iminoethanol and the sum of carbonyls are reduced by a factor of 4 and 6, respectively, in Bergen and Takle, compared to Mongstad. Modalen is least impacted by the PCCP plume and concentrations of all oxidation products are roughly one order of magnitude lower than in Mongstad. An exception is isocyanic acid which shows similar concentrations at all sites (0.09–0.20 ng m^{-3}). Isocyanic acid concentrations are slightly higher (by 30%) in Bergen and Takle, compared to Mongstad. Thus isocyanic acid, as a final oxidation product, becomes more important with increasing distance from the PCCP, both in relative terms of the product distribution and in absolute terms of ground-level concentrations.

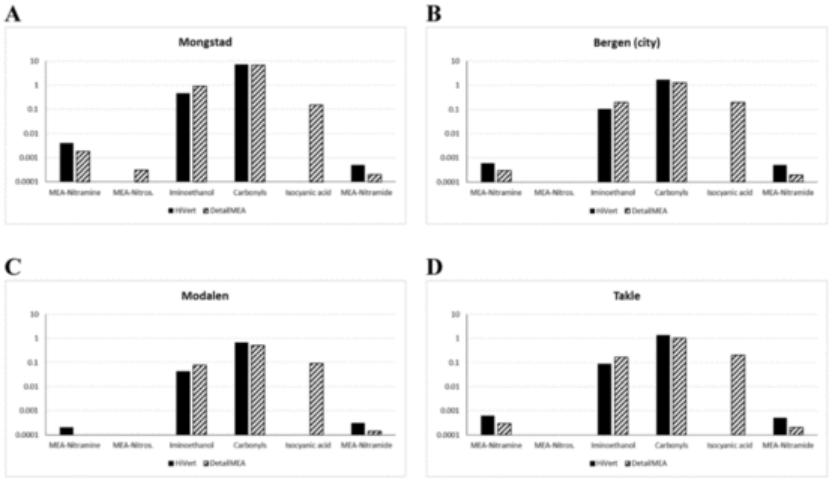

Fig. 7 Product distributions: simplified vs. detailed MEA chemistry, including MEA-nitramine, MEA-nitrosamine, sum Carbonyls, iminoethanol, isocyanic acid, and N-nitro hydroxyacetamide (here short as MEA-nitramide). Monthly mean air ~~concentration~~ concentrations (in ng m^{-3}) are shown on a logarithmic scale to facilitate the comparison of the concentration range, spanning five orders of magnitude.

In summary, the main differences of MEA-related oxidation products in simulation DetailMEA compared to simulation HiVert, in terms of grid maximum, grid average, and receptor sites, is the doubling of iminoethanol concentrations and the halving of MEA-nitramine concentrations. In order to understand the reasons for this discrepancy, the formation of these compounds in the plume from the PCCP was analysed. Vertical cross-sections of the plume (altitude vs. downwind distance) of monthly mean MEA-nitramine and iminoethanol concentrations up to 20 km downwind of the PCCP, calculated in the two WRF–Chem simulations, are shown in Fig. 8. Maximum production of MEA-nitramine and iminoethanol takes place in ca. 150–300 m height above Mongstad. The plume (on monthly average) reaches the ground in about 3–15 km distance from the PCCP. Along the plume cross-section, the discrepancies between DetailMEA and HiVert remain constant, i.e. factor 2 lower MEA-nitramine and factor 2 higher iminoethanol are consistently found in all grid cells influenced by the plume. One question was, if emitted MEA can influence the background chemistry in the vertical column over Mongstad. The faster reaction rate between MEA and OH given in the MEA-Detail scheme (20% higher than in MEA-Simple) indeed reduced OH levels in the vicinity of Mongstad by ca. 10% in heights up to 400 m in simulation DetailMEA compared to HiVert (not shown). However, NO_x levels and $[NO]/[NO_2]$ in the plume from both simulations were not significantly different (not shown), hence the discrepancy of a factor 2 in product concentrations cannot be explained by the non-linearity of O_3–HO_x–NO_x chemistry.

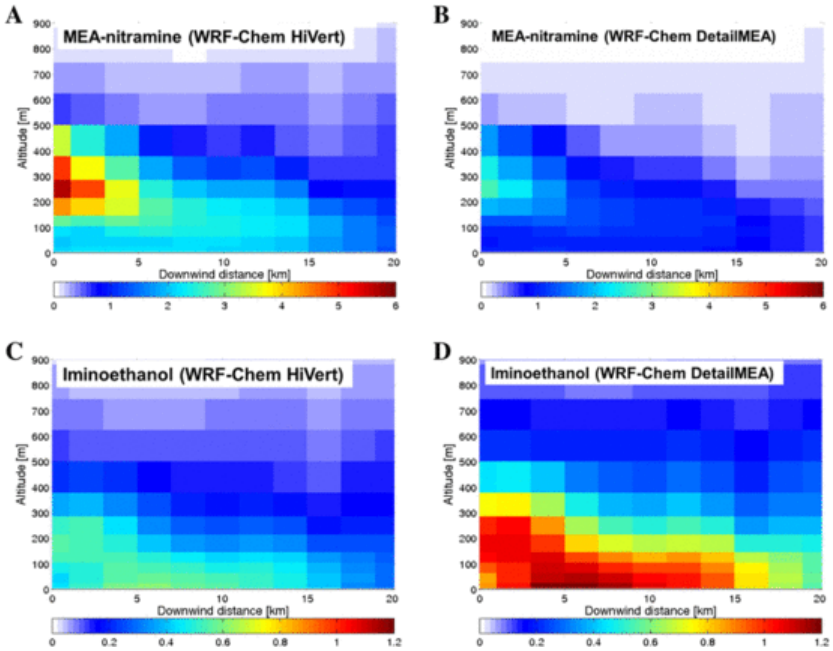

Fig. 8 Vertical cross-section of the plume (altitude – downwind distance) up to 20 km downwind of Mongstad from WRF-Chem calculations using MEA-Simple (simulation HiVert) and MEA-Detail (simulation DetailMEA). Monthly mean air concentration of (A) MEA-nitramine in pg m^{-3} (HiVert); (B) MEA-nitramine in pg m^{-3} (DetailMEA); (C) Iminoethanol in ng m^{-3} (HiVert); and (D) Iminoethanol in ng m^{-3} (DetailMEA). The plume axis was oriented in East–west direction, following the trajectory of highest monthly mean ground-level concentrations of MEA.

Therefore, the reason for the discrepancy lies in the differences of the parameterization of reactions following the H-abstraction at the $–NH_2$ group of MEA. In Table 4 the kinetic parameters of the branch starting with abstraction from the $–NH_2$-group in the MEA-Simple and MEA-Detail schemes are compared at a given $[NO]/[NO_2]$ ratio of 0.25 (The range of $[NO]/[NO_2]$ in the WRF-Chem simulation was 0.13 to 0.30 in a distance of up to 10 km downwind the PCCP). The initial branching at $–NH_2$ is 0.15 in MEA-Detail and 0.08 in MEA-Simple. The ratio of iminoethanol (IMIN) production and MEA-nitramine (MEN) production to the total production in the $–NH_2$ channel, respectively, are given by:

$$\frac{P_{IMIN}}{P_{TOT}} = \frac{k_4[O_2] + k_{3b}[NO_2]}{k_2[NO] + k_3[NO_2] + k_4[O_2]} \quad (1)$$

$$\frac{P_{MEN}}{P_{TOT}} = \frac{k_{3a}[NO_2]}{k_2[NO] + k_3[NO_2] + k_4[O_2]}. \quad (2)$$

Now the change in production between MEA-Detail and MEA-Simple can be derived by dividing the ratios P_{IMIN}/P_{TOT} (or P_{MEN}/P_{TOT}) of the two schemes and multiplication with the ratio of the initial branching (0.15/0.08). With the parameter values given in Table 4, the iminoethanol production is calculated to increase by a factor of 1.89 while the nitramine production is calculated to decrease by a factor of 0.43 when using MEA-Detail instead of MEA-Simple. This explains the factor two difference for both compounds. The change in production is further modulated by 10–20% due to the different rate constant of the MEA + OH reaction (k_1 is 20% higher in MEA-Detail) and different levels of [OH] in the two WRF-Chem simulations.

3.5 Effect of NO_x on formation of hazardous products

The sensitivity of atmospheric concentrations of hazardous products from the transformation of MEA in air towards changes in ambient NO_x mixing ratios was tested by removing NO_x emissions from the refinery at Mongstad in WRF-Chem simulation NoRefNOx (see vertical NO_x emission profile in Table 3). Monthly mean NO_x mixing ratios in the vertical cross-section of the plume up to a height of 900 m were reduced compared to WRF-Chem simulation DetailMEA (Figure S3A). Pronounced reduction of NO_x is found in the vertical column over Mongstad with a maximum of 4.2 ppb in the layer at 380–500 m height. In a height of 300–700 m NO_x mixing ratios were reduced by more than 0.5 ppbv up to a downwind distance of 6 km. In the model layer close to the ground below 100 m a reduction by 1.2–1.8 ppbv is evident 8–14 km downwind of Mongstad. Due to the non-linearity of the O_x–HO_x–NO_x chemistry, the NO_x reduction caused an increase of the OH concentration in the plume cross-section (Fig. S3B). The maximum OH increase by 0.7 × 10^6 cm^{-3} coincides with the maximum NO_x reduction in the layer at 380–500 m over Mongstad. Since both DetailMEA and NoRefNOx simulations use the MEA-Detail oxidation scheme, changes in the formation of MEA oxidation products are solely due to changes in modelled NO_x and OH concentrations. However, in the 3D-model the product concentration is spatially decoupled from the NO_x regime in which the products were initially formed since transport is faster than reaction between MEA and OH. The MEA + OH reaction rate increased due to increased OH concentrations: monthly mean reacted MEA at ground-level in the 40 × 40 km^2 study region was on average 10% higher in simulation NoRefNOx than in DetailMEA (Table 6). As a consequence of

the higher MEA + OH reaction rate, monthly mean concentrations of iminoethanol, which mainly forms in the reaction of the N-aminoethanol radical with O_2 (the contribution of the reaction of N-aminoethanol radical with NO_2 is minor, see Table 4) increased substantially in the plume (Fig. S3C). Formation of MEA-nitramine and MEA-nitrosamine is limited by the available NO_x. Thus, the formation of the two hazardous compounds in simulation NoRefNOx was expected to be reduced in the areas with pronounced NO_x reduction, although this may partly be compensated by the higher production due to increased MEA + OH reaction rate. Monthly mean MEA-nitramine concentrations in the plume cross-section were overall decreased in NoRefNOx (Fig. S3D). However in some areas of the plume cross-section, such as close to the emission source (up to 8 km downwind) below 100 m height, MEA-nitramine increased by up to 40% compared to simulation DetailMEA. MEA-nitrosamine increased even more, by 20–60%. Modelled monthly mean NO_x mixing ratios in the lowest 100 m decreased from a range of 0.8–1.8 ppbv in DetailMEA to a range of 0.4–0.6 ppbv in NoRefNOx. At the same time, monthly mean OH concentration close to the ground increased slightly by 20–40%. Obviously, these conditions were favourable for the production of MEA-nitramine, indicating high non-linearity of the O_3–HO_x–NO_x chemistry. The modelled grid maximum ground-level concentration of MEA-nitramine and MEA-nitrosamine in simulation NoRefNOx increased by 25% and 33%, respectively, in the 40 × 40 km^2 study area compared to simulation DetailMEA (Table 6), consistent with the increase of the two compounds near the ground along the plume cross-section. On grid average, however, monthly mean MEA-nitramine concentrations decreased by 40% as consequence of the overall reduced NO_x emissions from Mongstad.

The sensitivity of modelled MEA-nitramine air concentrations to changes of the background chemistry was further inspected in the tropospheric 1-D column over Mongstad. Since emissions from the PCCP are described by a volume source with a base area of 2 × 2 km^2 in the model and not by a point source, it is cautioned that the resulting concentrations from this grid column are not representative for concentrations at the point source or its close vicinity (few hundred ~~meters~~metres). Due to the instantaneous volume mixing of the emissions from Mongstad in the model, emitted NO immediately reacts with O_3 to form NO_2 and O_2 near the source, while in a real plume from an elevated point source, emitted NO would not be converted to NO_2 in the early stages of plume dispersion. The reason for choosing the 1D column over Mongstad is that it showed the largest variations of NO_x and MEA-nitramine. The scatterplot of MEA-nitramine concentration versus NO_x mixing ratio (Fig. 9A) using hourly data of the two simulations DetailMEA (open circles) and NoRefNOx (crosses) taken from the 1-D column over Mongstad revealed maximum MEA-nitramine concentrations for most of the time at NO_x mixing ratios in the range of 1–5 ppbv. MEA-nitramine concentrations > 40 pg m^{-3} only occurred when NO_x mixing ratios exceeded 2 ppbv, indicating the importance of high NO_x conditions for the production of hazardous compounds from the atmospheric oxidation of MEA. The distribution of modelled hourly OH radical concentrations as function of NO_x had a relatively broad maximum between 0.1 and 2.0 ppbv NO_x (Fig. 9B) with OH concentrations frequently above 6 × 10^6 cm^{-3}. At 10 ppbv NO_x the OH concentration drops by about a factor of 10 below the maximum values due to the dominance of the reaction between NO_2 and OH. Hourly NO_x levels in the range between 1 and 3 ppbv can be considered as favourable for the production of nitramines and nitrosamines in the boundary layer in the study region.

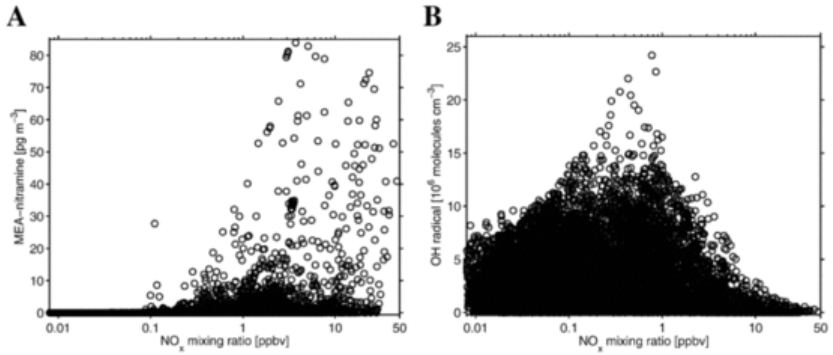

Fig. 9 Scatter plot of hourly modelled air concentration versus NO_x mixing ratio (in ppbv) in the tropospheric 1-D column over Mongstad in July 2007: (A) MEA-nitramine concentration (ng m^{-3}), and (B) OH radical concentration (10^6 cm^{-3}). Shown is the range of NO_x mixing ratios from 0.01 ppbv to 50 ppbv. Total number of data points (simulations DetailMEA and NoRefNOx) is 30,996.

4 Discussion

4.1 Model comparison and sensitivity analysis

The present evaluation of the health impact using the WRF–Chem model does not extend beyond prediction of air concentrations of hazardous products that form in the atmospheric oxidation. However, by comparison with the WRF–EMEP model, which can be coupled offline to the multimedia fugacity level III model (Karl et al., 2014), the results obtained from the WRF–Chem model can be used to evaluate the assumptions involved in the assessment of the environmental impact in air, soil and water. By comparison of results from the WRF–Chem model and the WRF–EMEP model, for identical horizontal and vertical resolution and identical meteorological input data, model-to-model differences with respect to the atmospheric oxidation of MEA were identified. WRF–Chem showed higher reactivity of MEA than WRF–EMEP, mainly due to higher O_3 levels and higher production of OH radicals at night. WRF–Chem uses 6-hourly ICs and BCs of chemical compounds from the CTM2 Oslo model, whereas WRF–EMEP uses climatological O_3 values as boundaries to the outer European domain. Reactions of various alkenes with O_3 as a source of OH radicals at night were included in RACM (used in WRF–Chem) leading to significant production of OH at night. Since MEA emissions from the PCCP occur day and night, the presence of OH with detectable concentrations at night are relevant for the formation of hazardous compounds.

In the present study, three aspects of the WRF–EMEP model framework (Karl *et al.*, 2014) were studied in sensitivity tests with the WRF–Chem model: (1) the description of the atmospheric oxidation of MEA; (2) the vertical resolution of the atmospheric

boundary layer; and (3) the effect of reduced NO_x emissions.

Increasing the vertical resolution from originally 20 model layers to 37 model layers affected modelled MEA-nitramine concentrations at the ground-level and at a height of 400–500 m. On average MEA-nitramine concentration at ground-level was decreased by 21% in the study region, probably due to stronger vertical mixing, when increasing vertical resolution. The change of direction of horizontal winds with increasing altitude was better resolved with a higher number of layers. This was found to be the most important effect of the increased vertical resolution since the changed wind direction affected the plume dispersion at several hundred ~~meter~~ metre height.

The effect of a more comprehensive oxidation scheme of MEA (MEA-Detail, developed by Karl et al., 2012) including more details on the formation of carbonylic compounds than the previously used simplified scheme MEA-Simple, was tested in further WRF-Chem simulations. Formamide and formaldehyde are the major carbonylic product forming in the atmospheric photo-oxidation of MEA (Nielsen et al., 2010; 2011). WRF-Chem predicted that formamide contributes about 70% to the ambient concentration of carbonyls (not including formaldehyde) from photo-oxidation of MEA emitted from a fictive full-scale PCCP. Atmospheric oxidation of emitted MEA resulted in calculated monthly mean ground-level concentrations of formamide and HNCO of up to 7.5 ng m^{-3} (about 4 pptv) and 0.4 ng m^{-3} (about 0.2 pptv), respectively, in this work.

The present study revealed a discrepancy in the parameterization of the gas-phase chemical formation mechanism of MEA-nitramine used in current models for assessing the health risk of amines. MEA-nitramine forms in the H-abstraction at the $-NH_2$ group of MEA leading to the N-amino radical. The rate k_{3a}·[NO_2] for the reaction of the N-amino radical to give MEA-nitramine in the scheme MEA-Detail (Karl et al., 2012) was found to be four times smaller than in the scheme MEA-Simple. MEA-Simple, which has been applied in the WRF-EMEP model framework, uses rate constant k_{3a} with a value determined by Lazarou et al. (1994) for the reaction of the dimethyl amino radical with NO_2. MEA-Detail on the other hand, which uses k_{3a} as reported by Nielsen et al. (2010), has been evaluated in EUPHORE chamber experiments (Karl et al., 2012). However, MEA-nitramine concentrations measured in the EUPHORE chamber experiments were associated with an uncertainty of a factor of three, preventing successful discrimination between the two k_{3a} rate constant values. In the comparison between MEA-Simple and MEA-Detail the discrepancy of the rate constant k_{3a} is partly compensated by different branching ratios used for the initial branching at the $-NH_2$ group, leading to a combined uncertainty of factor two for the prediction of atmospheric MEA-nitramine concentrations. The impact assessment using the WRF-EMEP model framework showed that a doubling of the MEA-nitramine production yield (from 8% to 16%) in the photo-oxidation of MEA causes an increase of the maximum drinking water concentration of the sum of nitrosamines and nitramines by 75% (Karl et al., 2014).

Reducing NO_x emissions from the Mongstad industrial area from 1930 to 90 tonnes per year caused a decrease of modelled MEA-nitramine air concentrations in the 40 × 40 km^2 study area by 40% on average. MEA-nitramine air concentration in the Mongstad grid cell increased by 25% due to increased OH concentrations close to the source.

4.2 Relevance for the health risk assessment

The health risk assessment for the CO_2 Technology Centre Mongstad (de Koeijer et al., 2013 (The reference to de Koeijer et al., 2013 is missing:

de Koeijer G, Talstad VR, Nepstad S, Tønnesen D, Falk-Pedersen O, Maree Y, Nielsen C. Health risk analysis of emissions to air from CO2 Technology Center Mongstad. Int J Greenhouse Gas Control 2013; 18: 200-7.
)) used a production yield of less than 0.3% for MEA-nitramine in the reaction of MEA with OH to calculate the average chemical conversion along the trajectory of maximum concentrations from the PCCP to the area of maximum impact, independent of NO_x levels along the trajectory. The WRF-EMEP model system, which took into account the spatial and temporal variability of levels of OH, NO, and NO_2, resulted in an average production yield of 0.9% (Karl et al., 2014). Results with WRF-Chem for July indicate a production yield of 0.1%, a factor of 9 lower than WRF-EMEP, due to lower ambient levels of NO_2 in WRF-Chem simulations. However, the increased reactivity of MEA in WRF-Chem resulted in similar average ground-level air concentrations of MEA-nitramine as in WRF-EMEP. Since the actual production rate of MEA-nitramine in air depends on the local concentration of MEA, on OH levels and on the availability of NO_2 the actual production yield is highly variable during the plume dispersion.

Isocyanic acid can cause protein carbamylation, a key step in the inflammatory response, linking to cardiovascular disease, rheumatoid arthritis and atherosclerosis (Roberts et al., 2011, and references therein). Ambient isocyanic acid mixing ratios of typically 100 pptv have been measured (Roberts et al., 2013), while mixing ratios above 1 ppbv were found in the plumes from biomass burning or in regions impacted by domestic wood burning and wild fires (Young et al., 2012; Roberts et al., 2013). Several countries regulate the occupational exposure from isocyanates but no explicit guidelines exist for the ambient health risk. A limit value of 1 ppbv has been tentatively used as guideline for ambient exposure since at this concentration protein carbamylation in vitro has been reported (Roberts et al., 2011). Roberts et al. (2013) estimated that formamide mixing ratios of about 30 pptv would be sufficient to explain ambient isocyanic acid mixing ratios of 100 pptv when assuming steady state with heterogeneous removal. Modelled formamide concentrations at Mongstad by WRF-Chem correspond to about 1/7 of the concentration estimate by Roberts et al. (2013). Thus the MEA emissions from a full-scale PCCP have the potential to slightly modify local and regional background levels of isocyanic acid. Further it was found in the WRF-Chem simulations that formation of isocyanic acid in the photo-oxidation of MEA, as a long-lived gas-phase product, becomes more important with increasing distance from the PCCP, both in relative terms of the product distribution and in absolute terms of ground-level concentrations.

4.3 CO_2-capture process emissions of nitrosamines and nitramines

Nitrosamines and nitramines are also formed through the degradation of amines within the absorption process in a post-combustion capture plant using amine solvents (Maree et al., 2013) with subsequent emission to air. Fostås et al. (2011) studied flue gas degradation of MEA as a function of O_2, NO_x and temperature in a solvent test rig and found that MEA degraded under the influence of NO_x to form the secondary amine diethanolamine (DEA) which is then nitrosated in aqueous solution. N-nitroso diethanolamine (NDEA) was the most prevalent nitrosamine found in wash-water from CO_2 capturing process plants using a MEA-based solvent (Dai et al., 2012). According to Dai et al. (2012) detected nitrosamine concentrations in wash-water would require a

factor of 16–000 reduction between the wash-water unit and the downwind water supplies, either by atmospheric dispersion or by reduction technology, in order to comply with the permit limit for TCM. However, photolysis of nitrosamines during daytime would rapidly degrade the nitrosamine and lower the required reduction factor. Emission of nitrosamines of 3.4 x *10^{-4} g s^{-1} corresponding to ca. 0.3% of the emitted MEA were estimated for the TCM capture plant when using flue gas from the combined heat and power plant (de Koeijer et al., 2013). The recent health risk study by Zhang et al. (2014) applied nitrosamine emissions for a MEA-based full-scale capture plant that were two orders of magnitude higher than in the TCM study. Unfortunately, reliable information on direct emissions of nitrosamines and nitramines from full-scale CO_2 capture is currently not published and therefore these emissions were not included in the present health risk assessment.

4.4 Comparison with environmental concentrations of MEA

Modelled monthly mean MEA concentrations in ground-level air 3 km downwind of the capture plant in the present study were in the range 14–20 ng m^{-3}. Since the full-scale CO_2 capture plant of this study is fictive it was not possible to compare with measured MEA concentrations. Background air concentrations of MEA in weekly samples taken at Mongstad were below 0.01 ng m^{-3} (Tønnesen et al., 2011). MEA concentrations of 0.2–1.86 μg L^{-1} were reported for Norwegian lakes (Poste et al., 2014). MEA concentrations in freshwater from the Mongstad area were below detection limit (de Koeijer et al., 2013). The risk of adverse environmental effects of amines in surface water is related to their potential nitrosation by reactions between precursor amines and oxidants such as nitrite (NO_2^-) in the aqueous phase (Poste et al., 2014). Relatively low concentrations of amines (nano-molar range) were found in fog water samples taken at two sites in the Mongstad area (Wang et al., 2015). NDMA in fog water detected at levels corresponding to gas-phase concentrations of 50 pg m^{-3} based on equilibrium partitioning (Wang et al., 2015) need to be considered with caution due to possible supersaturation in the fog droplets.

5 Conclusions

The reactivity of MEA in the study region was overall higher in the WRF–Chem simulations than predicted by the WRF–EMEP model framework presented in Karl et al. (2014). However, due to lower NO_x levels in WRF–Chem, the average production yield of MEA-nitramine in the reaction between MEA and OH was only 0.1%, a factor of 9 lower than in WRF–EMEP. Increasing the vertical resolution from 20 to 37 model layers decreased modelled MEA-nitramine concentration at ground-level by 21% in the study region. Reducing NO_x emissions from the Mongstad industrial area from 1930 to 90 tonnes per year decreased modelled MEA-nitramine concentration at ground-level by 40%. The production rate of MEA-nitramine from a new MEA oxidation scheme (Karl et al., 2012) was a factor of two lower than in a simplified MEA chemistry scheme, pointing to uncertainties in the kinetic parameters. The uncertainty associated with the formation of MEA-nitramine can only be further reduced by improving the measurement accuracy for nitramines in chamber photo-oxidation experiments. Predicted maximum air concentration of MEA-nitramine was found to critically depend on ambient NO_x mixing ratios. Hourly MEA-nitramine peak concentrations higher than 40 pg m^{-3} did only occur when NO_x mixing ratios were above 2 ppbv. Therefore, the spatial and temporal variability of levels of OH, NO, and NO_2 need to be taken into account in the health risk assessment. The further development of a model framework for the health risk assessment of amines emitted from CCS should focus on the following model aspects: (1) high vertical resolution of the atmospheric boundary layer; (2) detailed treatment of the photo-oxidation of amines including the formation of isocyanic acid; and (3) direct emission of nitrosamines, nitramines, and formamide. The use of hybrid coordinates has been initiated in the EMEP model allowing for flexible vertical resolution (Tsyro et al., 2014). Direct emissions should be included in future assessment studies for full-scale CO_2 capture, when a larger number of accurate emission measurements become available.

Acknowledgements

Philipp Schneider (NILU) is thanked for providing OMI satellite data on tropospheric NO_2 columns. We thank Øyvind Hodnebrog (CICERO) for assistance with his emission database program programme for WRF–Chem (version 3.4). Steinar Pedersen (Statoil AS) is thanked for critical remarks. We acknowledge the financial support from the Research Council of Norway, Statoil Petroleum AS, Shell, and Vattenfall under projectgrant 199874 (ExSIRA, Part C). The authors also thank NILU for additional financial support.

Appendix A. Supplementary data

Supplementary data to this article can be found online at http://dx.doi.org/10.1016/j.scitotenv.2015.04.108.

References

Atkinson RR. and Arey J., Gas-phase tropospheric chemistry of biogenic volatile organic compounds: a review, *Atmos. Environ.* (Suppl. No. 2), 2003, S197–S219.

Barnard J.C., Chapman E.G., Fast J.D., Schemlzer J.R., Slusser J.R. and Shetter R.E., An evaluation of the FAST-J photolysis algorithm for predicting nitrogen dioxide photolysis rates under clear and cloudy sky conditions, *Atmos. Environ.* **38**, 2004, 3393–3403.

Barnes I., Solignac G., Mellouki A. and Becker K.H., Aspects of the atmospheric chemistry of amides, *Chem. Phys. Chem.* **11**, 2010, 3844–3857.

Borduas N., Abbatt J.P.D. and Murphy J.G., Gas-phase oxidation of monoethanolamine (MEA) with OH radical and ozone: kinetics, products, and particles, *Environ. Sci. Technol.* **47**, 2013, 6377–6383.

California EPA, Public Health Goal for N-nitrosodimethylamine in Drinking Water, 2006, California Environmental Protection Agency, Pesticide and Environmental Toxicology

Branch, (http://oehha.ca.gov/water/phg/pdf/122206NDMAphg.pdf, (accessed December 10, 2014)).

Chen F. and Dudhia J., Coupling an advanced land–surface–hydrology model with the Penn State-NCAR MM5 modeling system. Part I: model implementation and sensitivity, *Mon. Weather Rev.* **129**, 2001, 569–585.

Dai N., Shah A.D., Hu L., Plewa M.J., McKague B. and Mitch W.A., Measurement of nitrosamine and nitramines formation from NO_x reactions with amines during amine-based carbon dioxide capture for postcombustion carbon sequestration, *Environ. Sci. Technol.* **46**, 2012, 9793–9801.

Dee D.P., Uppala S.M., Simmons A.J., Berrisford P., Poli P., Kobayashi S., Andrae U., Balmaseda M.A., Balsamo G., Bauer P., Bechtold P., Beljaars A.C.M., van de Berg L., Bidlot J., Bormann N., Delsol C., Dragani R., Fuentes M., Geer A.J., Haimberger L., Healy S.B., Hersbach H., Hólm E.V., Isaksen L., Kållberg P., Köhler M., Matricardi M., McNally A.P., Monge-Sanz B.M., Morcrette J.-J., Park B.-K., Peubey C., de Rosnay P., Tavolato C., Thépaut J.-N. and Vitart F., The ERA-Interim reanalysis: configuration and performance of the data assimilation system, *Q. J. R. Meteorol. Soc.* **137** (656), 2011, 553–597.

Fjellsbø L.M.B., Verstraelen S., Kazimirova A., Van Rompayb A.R., Magdolenova Z. and Dusinska M., Genotoxic and mutagenic potential of nitramines, *Environ. Res.* **134**, 2014, 39–45, http://dx.doi.org/10.1016/j.envres.2014.06.008.

Fostås B., Gangstad A., Nenseter B., Pedersen S., Sjøvoll M. and Sørensen A.L., Effects of NO_x in the flue gas degradation of MEA, *Energy Procedia* **4**, 2011, 1566–1573.

Frei E., Pool B.L., Plesch W. and Wiessler M., Biochemical and biological properties of prospective N-nitrodialkylamine metabolites and their derivatives, *IARC Sci. Publ.* **57**, 1984, 491–497.

Ge X., Wexler A.S. and Clegg S.L., Atmospheric amines – — part I: a review, *Atmos. Environ.* **45**, 2011, 524–546.

German drinking water ordinance, TrinkwV – — Ordinance on the Quality of Water for Human Use of 21.05.2001, *Federal Law Gazette* **vol. I**, 2001, 959.

Goodall C.M. and Kennedy T.H., Carcinogenicity of dimethylnitramine in NZR rats and NZO mice, *Cancer Lett.* **1**, 1976, 295–298.

Government of Ontario, Safe Drinking Water Act. Ontario Regulation 169/03, Schedule 2, 2002.

Grell G.A. and Devenyi D., A generalized approach to parameterizing convection combining ensemble and data assimilation techniques, *Geophys. Res. Lett.* **29** (14), 2002, 1693, http://dx.doi.org/10.1029/2002GL015311.

Grell G.A., Peckham S.E., Schmitz R., McKeen S.A., Frost G., Skamarock W.C. and Eder B., Fully coupled “online” chemistry within the WRF model, *Atmos. Environ.* **39**, 2005, 6957–6975.

Grosjean D., Atmospheric chemistry of toxic contaminants: 6. Nitrosamines: dialkyl nitrosamines and nitrosomorpholine, *J. Air Waste Manage. Assoc.* **41**, 1991, 306–311.

Guenther A., Hewitt C.N., Erickson D., Fall R., Geron C., Graedel T., Harley P., Klinger L., Lerdau M., McKay W.A., Pierce T., Scholes B., Steinbrecher R., Tallamraju R., Taylor J. and Zimmerman P., A global–model of natural volatile organic–compound emissions, *J. Geophys. Res.* **100**, 1995, 8873–8892.

Gustafson ~~W~~W.I., Jr., Fast ~~J~~J.D., Easter ~~R~~R.C. and Ghan ~~S~~S.J., Triumphs and tribulations of WRF-Chem development and use, Joint WRF/MM5 User's Workshop, June 27–30, 2005, Boulder, U.S.A., 2005.

Heikkilä U., Sandvik A. and Sorteberg A., Dynamical downscaling of ERA-40 in complex terrain using the WRF regional climate model, *Clim. Dyn.* **37** (7–8), 2011 (Please replace with"2010"), 1551–1564.

Hodnebrog ~~Ø~~Ø., Solberg ~~S~~S., Stordal ~~F~~F., Svendby ~~TM~~T.M., Simpson ~~D~~D., Gauss ~~M~~M., Hilboll ~~A~~A., Pfister ~~GG~~G.G., Turquety ~~S~~S., Richter ~~A~~A., Burrows ~~JP~~J.P. and Denier van der Gon ~~HAC~~H.A.C., Impact of forest fires, biogenic emissions and high temperatures on the elevated Eastern Mediterranean ozone levels during the hot summer of 2007, *Atmos. Chem. Phys.* **12**, 2012, 8727–8750, http://dx.doi.org/10.5194/acp-12-8727-2012.

Hong ~~S-Y~~S.-Y., Lim ~~K-SS~~K.-S.S., Lee ~~Y-H~~Y.-H., Ha ~~J-C~~J.-C., Kim ~~H-W~~H.-W., Ham ~~S-J~~S.-J. and Dudhia J., Evaluation of the WRF double-moment 6-class microphysics scheme for precipitation convection, *Adv. Meteorol.* **2010**, 2010, 707253, http://dx.doi.org/10.1155/2010/707253.

Iacono M.J., Delamere J.S., Mlawer E.J., Shephard M.W., Clough S.A. and Collins W.D., Radiative forcing by long-lived greenhouse gases: calculations with the AER radiative transfer models, *J. Geophys. Res.* **113**, 2008, D13103, http://dx.doi.org/10.1029/2008JD009944.

IARC, Some N-nitroso compounds, IARC (WHO International Agency for Research on Cancer), *Monographs on the Evaluation of the Carcinogenic Risks to Humans* **17**, 1982, 125–175.

IPCC., Climate change 2014: synthesis report, In: Pachauri R.K. and Meyer L.A., (Eds.), *Contribution of Working Groups I, II and III to the Fifth Assessment Report of the Intergovernmental Panel on Climate Change [Core Writing Team],* 2014,

IPCC; Geneva, Switzerland, (151 pp).

Janjic ZZ.I., Nonsingular implementation of the Mellor–Yamada Level 2.5 scheme in the NCEP Meso Model, NCEP Office Note No. 437, 2002, (61 pp).

Karl M., Wright R.F., Berglen T.F. and Denby B., Worst case scenario study to assess the environmental impact of amine emissions from a CO_2 capture plant, *Int. J. Greenhouse Gas Control* **5**, 2011, 439–447.

Karl M., Dye C., Schmidbauer N., Wisthaler A., Mikoviny T., D'Anna B., Müller M., Borrás E., Clemente E., Muñoz A., Porras R., Ródenas M., Vázquez M. and Brauers T., Study of OH-initiated degradation of 2-aminoethanol, *Atmos. Chem. Phys.* **12**, 2012, 1881–1901, http://dx.doi.org/10.5194/acp-12-1881-2012.

Karl M., Castell N., Simpson D., Solberg S., Starrfelt J., Svendby T., Walker S.-E. and Wright R.F., Uncertainties in assessing the environmental impact of amine emissions from a CO_2 capture plant, *Atmos. Chem. Phys.* **14**, 2014, 8533–8557, http://dx.doi.org/10.5194/acp-14-8533-2014.

Koorneef J., Ramírez A., Turkenburg W. and Faaij A., The environmental impact and risk assessment of CO_2 capture, transport and storage – – an evaluation of the knowledge base, *Prog. Energy Combust. Sci.* **38**, 2012, 62–86.

Kuenen JJ., Denier van der Gon HH., Visschedijk AA. and van der Brugh HH., High resolution European emission inventory for the years 2003–2007, In: *TNO report TNO-060-UT-2011-00588,* 2011, TNO; Utrecht, Netherlands.

Lazarou Y.G., Kambanis K.G. and Papagiannakopoulos P., Gas phase reactions of $(CH_3)_2$ N radicals with NO and NO_2, *J. Phys. Chem.* **98**, 1994, 2110–2115.

Lee D. and Wexler A.S., Atmospheric amines - part III: Photochemistry and toxicity, *Atmos. Environ.* **71**, 2013, 95–103.

Lepaumier H., Picq D. and Carrette P.L., Degradation study of new solvents for CO_2 capture in post-combustion, *Energy Procedia* **1** (1), 2009, 893–900.

Lepaumier H., da Silva E.F., Einbu A., Grimstvedt A., Knudsen J.N., Zahlsen K. and Svendsen H.F., Comparison of MEA degradation in pilot-scale with lab-scale experiments, *Energy Procedia* **4**, 2011, 1652–1659.

Loeppky R.N. and Michejda C.J., *Nitrosamines and Related N-Nitroso Compounds* **vol. 553**, 1994, American Chemical Society; Washington DC.

Maree Y., Nepstad S. and de Koeijer G., Establishment of knowledge base for emission regulation for the CO_2 Technology Centre Mongstad, *Energy Procedia* **37**, 2013, 6265–6272.

Morrison H., Thompson G. and Tatarskii V., Impact of cloud microphysics on the development of trailing stratiform precipitation in a simulated squall line: comparison of one- and two-moment schemes, *Mon. Weather Rev.* **137** (3), 2009, 991–1007.

Nielsen GJC.J., D'Anna BB., Dye GC., George GC., Graus MM., Hansel AA., Karl MM., King SS., Musabila MM., Müller MM., Schmidbauer NN., Stenstrøm YY. and Wisthaler AA., Atmospheric degradation of amines, summary report: gas phase oxidation of 2-aminoethanol (MEA), In: *CLIMIT project no. 193438, NILU OR 8/2010,* 2010.

Nielsen C.J., D'Anna B., Dye C., Graus M., Karl M., King S., Musabila M., Müller M., Schmidbauer N., Stenstrøm Y., Wisthaler A. and Pedersen S., Atmospheric chemistry of 2-aminoethanol (MEA), *Energy Procedia* **4**, 2011, 2245–2252.

Nielsen C.J., Herrmann H. and Weller C., Atmospheric chemistry and environmental impact of the use of amines in carbon capture and storage (CCS), *Chem. Soc. Rev.* **41**, 2012, 6684–6704.

NIPH, Health effects of amines and derivatives associated with CO_2 capture, In: Låg MM., Lindeman BB., Instanes GC., Brunborg GG. and Schwarze PP., (Eds.), 2011, Norwegian Institute of Public Health, (http://www.fhi.no/dokumenter/ca838717be.pdf, (accessed December 10, 2014)).

Onel L., Blitz M.A. and Seakins P.W., Direct determination of the rate coefficient for the reaction of OH radicals with monoethanol amine (MEA) from 296 to 510 K, *J. Phys. Lett.* **3**, 2012, 853–856.

Poste A.E., Grung M. and Wright R.F., Amines and amine-related compounds in surface waters: a review of sources, concentrations and aquatic toxicity, *Sci. Total Environ.* **481**, 2014, 274–279.

Puxty G., Rowland R., Allport A., Yang Q., Bown M., Burns R., Maeder M. and Attalla M., Carbon dioxide post-combustion capture: a novel screening study of the carbon dioxide absorption performance of 76 amines, *Environ. Sci. Technol.* **43**, 2009, 6427–6433.

Rao A.B. and Rubin E.S., A technical, economic, and environmental assessment of amine-based CO_2 capture technology for power plant greenhouse gas control, *Environ. Sci. Technol.* **36**, 2002, 4467–4475.

Reynolds A.J., Verheyen T.V., Adeloju S.B., Meuleman E. and Feron P., Towards commercial scale postcombustion capture of CO2 with monoethanolamine solvent: key considerations for solvent management and environmental impacts, *Environ. Sci. Technol.* **46**, 2012, 3643–3654.

Roberts J.M., Veres P.R., Cochran A.K., Warneke C., Burling I.A., Yokelson R.J., Lerner B., Gilman J.B., Kuster W.C., Fall R. and de Gouw J., Isocyanic acid in the atmosphere and its possible link to smoke-related health effects, *PNAS* **108** (22), 2011, 8966–8971.

Roberts J.M., Veres P.R., VandenBoer T.C., Warneke C., Graus M., Williams E.J., Lefer B., Brock C.A., Bahreini R., Öztürk F., Middlebrook A.M., Wagner N.L., Dubé W.P. and de Gouw J.A., New insights into atmospheric sources and sinks of isocyanic acid, HNCO, from recent urban and regional observations, *J. Geophys. Res.* **119**, 2013, 1060–1072, http://dx.doi.org/10.1002/2013JD019931.

Scherf H.R., Frei E. and Wiessler M., Carcinogenic properties of N-nitrodimethylamine and N-nitromethylamine in the rat, *Carcinogenesis* **10**, 1989, 1977–1981.

Shapley D., Nitrosamines: scientists on the trail of prime suspect in urban cancer, *Science* **191**, 1976, 268–270.

Simpson D., Benedictow A., Berge H., Bergström R., Emberson L.D., Fagerli H., Flechard C.R., Hayman G.D., Gauss M., Jonson J.E., Jenkin M.E., Nyíri A., Richter C., Semeena V.S., Tsyro S., Tuovinen J.-P., Valdebenito Á., The Wind P. and EMEP, MSC-W chemical transport model – technical description, *Atmos. Chem. Phys.* **12**, 2012, 7825–7865, http://dx.doi.org/10.5194/acp-12-7825-2012.

Skamarock W.C. and Klemp J.B., A time-split nonhydrostatic atmospheric model for weather research and forecasting applications, *J. Comput. Phys.* **227** (7), 2008, 3465–3485, http://dx.doi.org/10.1016/j.jcp.2007.01.037.

Søvde OA O.A., Gauss M M., Smyshlyaev SP S.P. and Isaksen ISA I.S.A., Evaluation of the chemical transport model Oslo CTM2 with focus on arctic winter ozone depletion, *J. Geophys. Res.* **113**, 2008, D09304, http://dx.doi.org/10.1029/2007JD009240.

Stockwell W.R., Kirchner F., Kuhn M. and Seefeld S., A new mechanism for regional atmospheric chemistry modelling, *J. Geophys. Res.* **102** (D22), 1997, 25847–25879.

Stohl A A., Forster C C. and Sodemann H H., Remote sources of water vapor forming precipitation on the Norwegian west coast at 60°N – a tale of hurricanes and atmospheric river, *J. Geophys. Res.* **113**, 2008, D05102, http://dx.doi.org/10.1029/2007JD009006.

Tang Y., Hanrath M. and Nielsen C.J., Do primary nitrosamines form and exist in the gas phase? A computational study of CH_3NHNO and $(CH_3)_2NNO$, *Phys. Chem. Chem. Phys.* **14**, 2012, 16365–16370.

Tønnesen Ð D., Dye C C. and Bøhler T T., Baseline study on air and precipitation quality for the CO_2 Technology Centre Mongstad, NILU Report OR 73/2011.NILU, Kjeller, Norway, 2011.

Tsyro S S., Karl M M., Simpson Ð D., Valdebenito A A. and Wind P P., Updates to the EMEP/MSC-W model, in: transboundary particulate matter, photo-oxidants, acidifying and eutrophying components, In: Fagerli H H., Schulz M M., Gauss M M., Tsyro S S., Jonson JE J.E., Benedictow A A., Simpson Ð D., Valdebenito A A., Griesfeller J J., Semeena VS V.S., Wind P P., Olivié Ð D., Aas W W., Hamburger T T., Hjellbrekke A-G A.-G., Solberg S S., Tørseth K K., Yttri K-E K.-E., Karl M M., Mareckova K K., Wankmüller R R., Alastuey A A., Posch M M. and Tuovinen J-P J.-P., (Eds.), *Norwegian Meteorological Institute – MSC-W (EMEP Status Report 1/2014), Oslo,* 2014, 143–146.

U.S. EPA, Health and environmental effects profile for nitrosamines, Prepared by the Office of Health and Environmental Assessment, 1986, Environmental Criteria and Assessment Office, Cincinnati, OH for the Office of Solid Waste and Emergency Response; Washington, DC.

Veltman K., Singh B. and Hertwich E.G., Human and environmental impact assessment of postcombustion CO_2 capture focusing on emissions from amine-based scrubbing solvents to air, *Environ. Sci. Technol.* **44**, 2010, 1496–1502.

Vevelstad S.J., Eide-Haugmo I., da Silva E.F. and Svendsen H.F., Degradation of MEA: a theoretical study, *Energy Procedia* **4**, 2011, 1608–1615.

Vieno M., Dore A.J., Stevenson D.S., Doherty R., Heal M.R., Reis S., Hallsworth S., Tarrason L., Wind P., Fowler D., Simpson D. and Sutton M.A., Modelling surface ozone during the 2003 heat-wave in the UK, *Atmos. Chem. Phys.* **10**, 2010, 7963–7978, http://dx.doi.org/10.5194/acp-10-7963-2010.

Wang Y., Zhang J., Marcotte A.R., Karl M., Dye C. and Herckes P., Fog chemistry at three sites in Norway, *Atmos. Res.* **151**, 2015, 72–81.

Wesely M.L., Parameterization of surface resistances to gaseous dry deposition in regional scale numerical models, *Atmos. Environ.* **23** (6), 1989, 1293–1304.

Wild O., Zhu X. and Prather M.J., Fast-J: accurate simulation of in- and below cloud photolysis in tropospheric chemical models, *J. Atmos. Chem.* **37**, 2000, 245–282.

Wingenter O., Kubo M., Blake N., Smith T., Jr., Blake D. and Rowland F., Hydrocarbon and halocarbon measurements as photochemical and dynamical indicators of atmospheric hydroxyl, atomic chlorine, and vertical mixing obtained during Lagrangian flights, *J. Geophys. Res.* **101** (D2), 1996, 4331–4340.

WRF ARW, http://www2.mmm.ucar.edu/wrf/users/tutorial/tutorial_presentation_winter_2014.htm 2014, (accessed December 10, 2014).

Young PJP.J., Emmons LKL.K., Roberts JMJ.M., Lamarque J-FJ.-F., Wiedinmyer CC., Veres PP. and VandenBoer TCT.C., Isocyanic acid in a global chemistry transport model: tropospheric distribution, budget, and identification of regions with potential health impacts, *J. Geophys. Res.* **117**, 2012, D10308, http://dx.doi.org/10.1029/2011JD017393.

Zhang Y., Xu J., Zhang Y., Zhang J., Li Q., Liu H. and Shang M., Health risk analysis of nitrosamine emissions from CO_2 capture with monoethanolamine in coal-fired power plants, *Int. J. Greenhouse Gas Control* **20**, 2014, 37–42.

Appendix A. Supplementary data

Multimedia Component 1

Supplementary material.

Graphical abstract

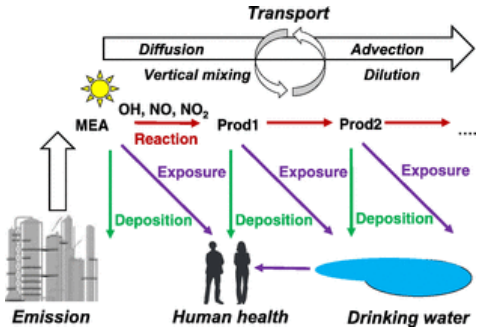

Highlights

- Amine emissions from full-scale CO_2-capture evaluated
- Predicted air concentrations of hazardous products at high spatiotemporal resolution
- Isocyanic acid relevant oxidation product on regional scale
- Ground-level concentration of nitramines sensitive to ambient NO_x

---

Queries and Answers

Query:

Please check the presentation of Tables 1-7 if correct and amend if necessary.

Answer: Made changes in: Table 3, 4, 6 and 7

Query:

Your article is registered as a regular item and is being processed for inclusion in a regular issue of the journal. If this is NOT correct and your article belongs to a Special Issue/Collection please contact a.louis@elsevier.com

immediately prior to returning your corrections.

Answer: Yes

Query:

Please confirm that given names and surnames have been identified correctly.

Answer: Yes

Query:

The citation "Veltman et al., 2011" has been changed to match the author name/date in the reference list. Please check here and in subsequent occurrences, and correct if necessary.

Answer: "Veltman et al., 2010" is correct

Query:

The citation "Shapley et al., 1976" has been changed to match the author name/date in the reference list. Please check here and in subsequent occurrences, and correct if necessary.

Answer: "Shapley, 1976" is correct

Query:

The citation "Skamarock et al., 2008" has been changed to match the author name/date in the reference list. Please check here and in subsequent occurrences, and correct if necessary.

Answer: "Skamarock and Klemp, 2008" is correct

Query:

The citation "Heikkilä et al. (2010)" has been changed to match the author name/date in the reference list. Please check here and in subsequent occurrences, and correct if necessary.

Answer: Should be "Heikkilä et al. (2010)". Corrected all occurences

Query:

The citation "Barnes et al., 2011" has been changed to match the author name/date in the reference list. Please check here and in subsequent occurrences, and correct if necessary.

Answer: "Barnes et al., 2010" is correct

Query:

The term "pptv" is also presented in the text as "ppbv". Please check if these should be made consistent, and amend as necessary.

Answer: The use of "pptv" is correct here (i.e. "parts per trillion").

Query:

Citation "de Koeijer et al., 2013" has not been found in the reference list. Please supply full details for this reference.

Answer: The reference is: de Koeijer G., Talstad V. R., Nepstad S., Tønnesen D., Falk-Pedersen O., Maree Y., and Nielsen C. Health risk analysis of emissions to air from CO2 Technology Center Mongstad. Int. J. Greenhouse Gas Control 2013; 18: 200-7.

Query:

Citation "de Koeijer et al., 2013" has not been found in the reference list. Please supply full details for this reference.

Answer: The reference is: de Koeijer G., Talstad V. R., Nepstad S., Tønnesen D., Falk-Pedersen O., Maree Y., and Nielsen C. Health risk analysis of emissions to air from CO2 Technology Center Mongstad. Int. J. Greenhouse Gas Control 2013; 18: 200-7.

Query:

Citation "de Koeijer et al., 2013" has not been found in the reference list. Please supply full details for this reference.

Answer: The reference is: de Koeijer G., Talstad V. R., Nepstad S., Tønnesen D., Falk-Pedersen O., Maree Y., and Nielsen C. Health risk analysis of emissions to air from CO2 Technology Center Mongstad. Int. J. Greenhouse Gas Control 2013; 18: 200-7.

Query:

The citation "Tsyro, 2014" has been changed to match the author name/date in the reference list. Please check here and in subsequent occurrences, and correct if necessary.

Answer: "Tsyro et al., 2014" is correct

Query:

Please provide the corresponding grant numbers for the grant sponsors "Research Council of Norway", "Statoil Petroleum AS", "NILU", and "Shell".

Answer: The grant number of "Research Council of Norway", "Statoil Petroleum AS", "Shell" and "Vattenfall" is the same. For "NILU" there is no grant number.

Query:

Supplementary caption was not provided. Please check suggested data if appropriate and correct if necessary,

Answer: This is ok